Received: 10 November 2022 | Revised: 3 April 2023 | Accepted: 17 April 2023

DOI: 10.1002/cne.25494

RESEARCH ARTICLE

JCN RESEARCH IN SYSTEMS NEUROSCIENCE THE JOURNAL OF COMPARATIVE NEUROLOGY WILEY

Naturally occurring histological findings and Alzheimer's-like pathology in the brain of aging African green monkeys (*Chlorocebus sabaeus*)

Tatiana M. Corey[1,2,3] | **Oscar Illanes**[1,5] | **Matthew Lawrence**[2,3] | **Sylvia E. Perez**[4] | **Shervin Liddie**[2,3] | **John J. Callanan**[1]

[1]Center for Integrative Mammalian Research, Ross University School of Veterinary Medicine, Basseterre, Saint Kitts and Nevis

[2]Virscio, Inc., New Haven, Connecticut, USA

[3]St. Kitts Biomedical Research Foundation, Basseterre, Saint Kitts and Nevis

[4]Department of Neurobiology, Barrow Neurological Institute, Phoenix, Arizona, USA

[5]Department of Veterinary Biomedical Sciences, Long Island University College of Veterinary Medicine, Brookville, New York, USA

Correspondence
Tatiana M. Corey, University of Texas Health at San Antonio, 7703 Floyd Curl Dr, San Antonio, TX 78229, USA.
Email: corey@uthscsa.edu

Funding information
Ross University School of Veterinary Medicine via the Center for Integrative Mammalian Research; Virscio, Inc.

Abstract

Nonhuman primates (NHPs) are important to study the pathophysiology of neurodegenerative disease and evaluate therapies targeting the central nervous system (CNS). Understanding the age-associated incidence of natural CNS pathology in a given NHP species is critical to assess the safety of potential treatments for neurodegenerative disorders like Alzheimer's disease (AD). We describe background and age-related neuropathology in the St. Kitts African green monkey (AGM), a recognized translational model for neurodegenerative research, additionally defining the age progression of AD-associated neuropathology in this species. Seventy-one AGM brains were examined, representing age groups of 3–6 years ($n = 20$), 7–9 years ($n = 20$), 10–15 years ($n = 20$), and >15 years ($n = 11$). A subset of brains ($n = 31$) was assessed immunohistochemically for AD-related pathology, including expressions of Aβ, tau, and GFAP. Age-related microscopic findings included hemosiderosis, spheroid formation, neuronal lipofuscinosis and neuromelanosis, white matter and neuropil vacuolation, astrocytosis, and focal microgliosis. Non-age-related findings included perivascular ceroid-laden macrophages, meningeal melanosis, and vascular mineralization. Immunohistochemistry revealed 4G8-immunopositive Aβ plaques and vascular deposits in the prefrontal, frontal, cingulate, and temporal cortices of nine animals over 15 years of age, with associated increase in GFAP expression. In 12 animals, 11 over the age of 10 years, phosphorylated tau CP13-immunoreactive neurons, neuropil, and oligodendrocyte-like cells were seen in the prefrontal, frontal, cingulate, orbital, temporal, and entorhinal cortices as well as the hippocampus; no neurofibrillary tangles were observed. AD-related pathology showed an age-related development in cognitive-associated areas in the AGM, highlighting the value of the AGM as a natural model for these neurodegenerative diseases.

KEYWORDS
African green monkey, aging, Alzheimer's disease, amyloid, animal model, neuropathology, nonhuman primate, tau

1 | INTRODUCTION

In biomedical research, knowledge of naturally occurring background histopathology is necessary for the selection and characterization of animal models and for the proper evaluation of drug safety studies. In particular, understanding naturally occurring age-related neuropathology in nonhuman primates (NHPs) is essential for the evaluation of the safety and efficacy of potential therapeutics for neurodegenerative disorders, like Alzheimer's disease (AD), a disorder characterized by the accumulation of amyloid-β (Aβ) plaques, neurofibrillary tangles (NFTs), and cognitive decline (Sanabria-Castro et al., 2017). Previous studies have described background neuropathology such as vacuolation, spheroid formation, lipofuscin and neuromelanin accumulation, blood vessel wall mineralization, and inflammatory changes in NHPs including rhesus and cynomolgus macaques and squirrel monkeys (Cork & Walker, 1993; Heuer et al., 2017; Hof et al., 2002; Sasseville et al., 2012), as well as other animal models. However, little is known about the background neuropathology of African green monkeys (AGMs), a species used as model for neurodegenerative disorders including AD.

Animal model research has been critical to the current understanding of AD pathophysiology. NHP models have played an essential role in the identification of potentially effective therapeutics for this neurodegenerative disorder. While many induced animal models of AD-associated neuropathology exist, naturally derived AD-associated pathology has best been described in NHP species including, but not limited to, great apes, baboons, rhesus and cynomolgus macaques, marmosets, squirrel monkeys, and the Saint Kitts AGM (*Chlorocebus sabaeus*) (Edler et al., 2017; Gearing et al., 1994; Heuer et al., 2017; Kimura et al., 2001; Ndung'u et al., 2012; Oikawa et al., 2010; Perez et al., 2013; Schultz et al., 2000). These superior animal models warrant further evaluations to determine the natural reproducibility of AD-associated neuropathology coupled with an understanding of the background neuropathology expected with age. Notably, AGM is a medium-sized Old World monkey with a captive life span over 30 years and is an invasive species in St. Kitts, where it is believed a population greater than 30,000 monkeys exist in the wild (Jasinska et al., 2012; Lemere et al., 2004; IUCN Red List of Threatened Species, 2022) making them of "Least Concern" conservation status. The isolated biogeography of St. Kitts has prevented exposure to common NHP pathogens including immunodeficiency-causing retroviruses (simian immunodeficiency virus, simian retrovirus, and simian T-cell leukemia virus), or any other known pathogenic viruses from their continental origin in Africa (e.g., simian hemorrhagic fever virus). Additionally, they are not carriers of the fatal Macacine herpesvirus 1 (Herpes B virus), a significant occupational health threat for investigators working with macaque species in biomedical research (Jasinska et al., 2012; Lemere et al., 2004). These qualities have made the AGM a valuable resource for medical and neurological research, including as a critical animal model for Parkinson's research (Collier et al., 2016; Elsworth et al., 2000; Horvath et al., 2003; Hurley et al., 2011; Lawrence et al., 1991; Taylor et al., 1991).

There is limited work published exploring the AD neuropathology in the AGMs during aging. Three prior AD research studies, which included just a few animals, demonstrated Aβ pathology in aged AGMs and verified the homozygous ApoE4 allele status of this species (Fainman et al., 2007; Kalinin et al., 2013; Lemere et al., 2004). More recent studies examined transcriptional, pathological, and cognitive changes in aged AGMs. Three of these examined animals ranging from 15 to 32 years of age. Cramer et al. (2018) identified 6E10-immunoreactive (ir) Aβ plaques in the cingulate sulcus, lateral fissure, entorhinal cortex (EC), and frontal cortex (FC) of ageing individuals. Kumar et al. (2018) also screened for phosphorylated and nonphosphorylated Aβ using pSer8Ab and npAb antibodies, respectively, detecting mild immunoreactivity for both antibodies in the FC of three middle-aged AGMs (11–15 years) and in the FC, temporal cortex (TC), and hippocampus, with pSer8Ab immunoreactivity in meningeal and parenchymal blood vessels, in eight aged AGMs (16–32 years). Latimer et al. (2018) also evaluated the aged AGM, identifying immunoreactivity for Aβ (6E10 antibody) and paired helical filaments (PHF; AT8 antibody) and finding higher Aβ plaques and PHF burden predictive for smaller brain volumes in certain cortical regions. Hyperphosphorylated tau has additionally been identified in the hippocampus and EC of two aged AGMs (<20 years old) using both Gallyas silver staining and AT8 antibody (Cramer et al., 2018). These tau findings support earlier descriptions of mild phospho-tau immunoreactivity without NFT formation in two aged AGMs (Lemere et al., 2004).

To our knowledge, background neuropathology in clinically normal AGMs has not been well-documented. To close this knowledge gap, here we describe age-related and non-age-related histopathological findings in 71 AGM brains, and further evaluate in a large group the age relationship of AD-associated pathology that naturally develops in the AGM. The present study represents the largest evaluation of AGMs for AD pathology to date ($n = 31$) performed across a wide age range (3–25 years) to investigate the time progression of these lesions in addition to a broader study of background neuropathology. These findings will provide the basis for interpreting future drug efficacy studies for AD or any drug studies where neuropathology assessment is required.

2 | MATERIALS AND METHODS

2.1 | Specimens and sampling

Brains from 71 AGMs were obtained from two St. Kitts biomedical research facilities. All monkeys were housed and maintained in compliance with "The Guide for the Care and Use of Laboratory Animals" and the U.S. Public Health Service's "Policy on Humane Care and Use of Laboratory Animals." Experiments were performed in accordance with approved institutional animal care and use committee protocols. In accordance with the 3R principles for animal research, brains were obtained from monkeys enrolled in experimental studies for which there was no expectation or evidence of an impact on the central

nervous system (CNS). Monkeys were euthanized with an overdose of pentobarbital (n = 67), except four aged monkeys that died of natural causes: one from acute gastrointestinal dilatation, and three from *Pasteurella multocida*-associated pleuritis and peritonitis. Animals underwent physical and neurologic examinations prior to study enrollment or prior to euthanasia, and no overt signs of neurologic disease were observed in any animal prior to euthanasia.

In this study, all monkeys, except for one, were wild caught. Wild-caught animal ages were estimated upon intake and again prior to necropsy by experienced veterinary staff using internally evaluated criteria including, but not limited to, dentition, skin elasticity, musculoskeletal changes, and genital and/or breast development (National Research Council., 1981). Seven of the aged animals had a verifiable age of over 19 years based on the year of facility intake, with age estimates ranging from 20 to 25 years; one captive-bred monkey had a known age of 25 years. These old monkeys demonstrated signs of aging that have been described in other NHP species: musculoskeletal changes including muscle wasting, joint stiffness, and kyphosis; coat roughening and hair loss; wrinkling and loose facial skin; tooth loss and wearing; and changes in voice timbre (National Research Council., 1981). To assess the age-related histopathologic changes, monkeys were divided into four groups (group 1: 3–6 years, n = 20, 10 M/10 F; group 2: 7–9 years, n = 20, 19 M/1 F; group 3: 10–15 years, n = 20, 16 M/4 F; group 4: >15 years, n = 11, 2 M/9 F).

Brains were collected immediately following euthanasia or within 8 h of death. All brains were fixed in 4% paraformaldehyde for 1–2 weeks at room temperature (RT) or 4°C, and were subsequently transferred to phosphate-buffered saline with 0.05% azide for storage at 4°C. All brains were collected over a period of 3 years. Fixed tissue trimmed at the level of the FC, basal ganglia, thalamus and hippocampus, pons, medulla oblongata at the level of the obex, and cerebellum was routinely processed and embedded in paraffin, cut into 4-μm coronal sections, mounted on glass slides, and stained with hematoxylin and eosin (H&E). When appropriate, special stains were performed including Von Koss for mineralization, Perl's Prussian blue for iron products including hemosiderin, Fontana Masson for melanin and neuromelanin, and carbol fuchsin long acid-fast stain for lipofuscin and ceroid.

2.2 | Histopathologic survey

Each H&E-stained section of the brain was systematically examined for pathological changes. During examination, the animal ID was concealed to reduce reviewer bias. For each tissue section, white matter (WM) vacuoles were counted in five representative high-power fields using a 10× objective, and arbitrarily graded as follows: grade 1, less than five vacuoles per field; grade 2, five to 15 vacuoles per field; grade 3, greater than 15 vacuoles per field. Similarly, neuropil vacuoles were counted using a 10× objective, and for the purpose of quantification, arbitrarily graded as follows: grade 1, less than five vacuoles observed per tissue section; grade 2, five to 10 vacuoles observed per tissue section; grade 3, more than 10 vacuoles observed per tissue section. Neuronal lipofuscin deposits were arbitrarily graded as follows: grade 1, less than 25% of neurons observed to contain lipofuscin per anatomical region; grade 2, 25–50% of neurons observed to contain lipofuscin per region; grade 3, more than 50% of neurons observed to contain lipofuscin per region (Jahns, Callanan, McElroy, et al., 2006). The presence and anatomical distribution of spheroids, hemosiderin, perivascular ceroid, intramural vascular mineralization, astrocytosis and gliosis, perivascular cuffing, melanin, and neuromelanin and any other microscopic findings were documented. Additionally, the presence of roughly round, pale eosinophilic aggregates, interpreted as Aβ plaques, in cerebral cortex neuropil was also documented (Serrano-Pozo et al., 2011).

2.3 | Immunohistochemistry

For immunohistochemical evaluation, 31 monkeys were grouped into four age-based groups (group 1: 3–6 years, n = 5, 2 M/3 F; group 2: 7–9 years, n = 5, 5 M/0 F; group 3: 10–15 years, n = 10, 6 M/4 F; group 4: >15 years, n = 11, 2 M/9 F).

A representative tissue section of the FC containing the prefrontal cortex (PFC), anterior cingulate cortex (CC), and orbital cortex (OC) and a second section of the temporal lobe (MTL) containing TC, posterior hippocampal formation, and EC were selected from each animal. Tissues were stained on an intelliPATH automated stainer from Biocare (Biocare Medical, Concord, CA, USA). All tissue sections were deparaffinized in xylene and hydrated in a series of degraded concentrations of ethanol (100%, 95%, 70%, and 50%). Tris-buffered saline (TBS) with Tween was used to rinse all tissues three times between each step described. Initial antigen retrieval was performed with incubation in boiling Diva Decloaker (Biocare) at 110°C for 15 min, then tissue was placed in Peroxidazed 1 to block endogenous peroxidase activity (5 min) at RT and Background Punisher blocking solution (10 min; RT). Tissues were then incubated in GA5 anti-GFAP mouse monoclonal antibody (1:2500, 1 h) (catalog #3670S, Cell Signaling Technology®, Danvers, MA, USA) or 4G8 anti-β-Amyloid, 17–24 antibody (1:5000; 1 h) (catalog #800701, Biolegend®, San Diego, CA, USA) at RT. Subsequently, tissues were incubated with Mouse on Farma HRP Polymer secondary antibody (30 min; RT) and Betazoid DAB (5 min; RT). Final steps included staining with Mayer's Hematoxylin counterstain (5 min; RT) for anatomical guidance, and all tissues were dehydrated, cleared in xylenes, and cover slipped. All slides were scanned using the Hamamatsu Nanozoomer slide scanner (Hamamatsu Photonics K.K., Hamamatsu City, Japan). Microscopic evaluation of digitized images of the scanned immunostained tissue slides was performed using Nanozoomer viewing software (NDP.view2 Plus, Hamamatsu Photonics K.K., Hamamatsu City, Japan). The presence of discrete extracellular Aβ accumulations in positive-stained regions was interpreted as Aβ plaques and quantified with their anatomical distribution documented. The presence and anatomic location of intramural vascular Aβ-immunoreactivity, as well as poorly defined extracellular areas of Aβ-immunoreactivity, were also documented. Three Aβ plaques per section were randomly selected and their diameter measured. All sections with Aβ plaques and intramural vascular accumulations were

compared to the adjacent GFAP-stained slides to identify possible increases of GFAP-immunoreactivity around Aβ plaques or intramural vascular accumulations.

Single immunostaining was performed using antibodies directed against the phosphorylated tau (p-tau) at serine 202 (CP13; gift from Peter Davies) and serine 202/threonine 205 (AT8, Invitrogen, Carlsbad, CA, USA). All sections were deparaffinized in xylene, hydrated in a series of degraded concentrations of ethanol (100%, 95%, 70%, and 50%), and pretreated with heated citric acid in a microwave (pH 6; 10 min). After several washes in TBS, sections were incubated in sodium metaperiodate (0.01 M) solution (20 min) to inactivate endogenous peroxidase activity, rinsed three times in TBS, and placed in blocking solution containing 0.25% Triton X-100/3% goat serum (GS) (1 h; RT) and then incubated with primary antibodies at 1:100 in a solution of TBS 0.25% Triton X-100/1% GS overnight at RT or two nights at 4°C. After several 1% GS TBS washes, tissue was incubated with a goat anti-mouse biotinylated secondary antibody (1:200; 1 h) (Vector Labs, Burlingame, CA, USA) as appropriate, incubated in Vectastain ABC kit (1 h) (Vector Labs), and developed in acetate–imidazole buffer containing 0.05% 3,3′-diaminobenzidine tetra hydrochloride (Thermofisher Scientific, Waltham, MA, USA) and 0.005% H_2O_2, resulting in a brown reaction product. Select sections were counterstained with Mayer's hematoxylin for anatomical guidance. All slides were dehydrated, cleared in xylenes, and cover slipped using DPX (Electron Microscopy Sciences, Hatfield, PA, USA). To control for batch-to-batch variation in immunostaining procedures, sections from each case were processed at the same time for each antibody. FC paraffin-embedded tissue from an 82-year-old female with neuropathologically confirmed AD (Braak NFT stage VI) was used as tau positive control. Primary antibody omission resulted in absence of immunostaining for each antibody. Reacted sections were photographed using a Nikon Eclipse 80i, and contrast and brightness were adjusted using Adobe Photoshop (Adobe, San Jose, CA, USA). Due to the limited positive immunostaining observed for both antibodies, the tau immunohistochemistry (IHC) was evaluated qualitatively, with the presence and anatomic location of positive immunostaining documented.

2.4 | Statistical analysis

Each histopathologic finding was evaluated by chi-square analysis, comparing by group the number of individuals in which the finding was identified to determine if the finding was "age related." Findings were described as "age related" if there was a statistically significant increase in the number of monkeys demonstrating the finding, compared between groups. Kruskal–Wallis test was used to evaluate the quantitative presence of WM vacuoles, neuropil vacuoles, and lipofuscin deposits, applying the grading schemes previously described to determine if findings were "age progressive." Findings were described as "age progressive" if the intensity of the finding increased across age groups. Immunohistochemical results were evaluated by chi-square analysis, comparing the presence of Aβ plaques, intramural vascular Aβ accumulations, and p-tau between groups to determine if findings were "age related," while one-way ANOVA with Tukey's HSD test for multiple comparisons was applied to compare the average number of Aβ plaques observed per group to determine if they were "age progressive." The statistical level of significance was set at $\alpha = .05$ for all tests (GraphPad Prism 9; GraphPad Software, San Diego, CA, USA).

3 | RESULTS

3.1 | Age-related histopathology

Histopathology results are summarized in Table 1 and Figure 4a. Perivascular and neuropil hemosiderin deposits and hemosiderin-laden macrophages were observed in 15 out of 71 brains, primarily in the diencephalon, including the thalamus, hypothalamus, and globus pallidus (Figure 1a). Specifically, we observed hemosiderosis in one group 2 animal, five group 3 animals, and nine group 4 animals. The number of monkeys displaying hemosiderosis increased significantly with age ($p < .0001$). It was often observed in conjunction with lipofuscin, intramural vascular mineralization, gliosis, and spheroids.

Swollen, roughly round, eosinophilic neuronal cell processes (20–60 μm) interpreted as spheroids were a common finding (Figure 1b). Spheroids were detected in 32 out of 71 brains including in monkeys as young as 3 years old; specifically, we observed spheroids in five group 1 animals, seven group 2 animals, nine group 3 animals, and all animals in group 4. Spheroids were significantly age related, as they were more likely to be found in older monkeys than young ($p = .0006$). Spheroids were observed in small clusters, frequently with a bilaterally symmetric distribution, most commonly within the gracile and cuneate nuclei, thalamus, and hypothalamus. In animals under 15 years old, over 70% of spheroids were confined to nuclei of the medulla oblongata, while in animals over 15 years old, spheroids were common in both the diencephalon (75%) and the medulla oblongata (25%). Spheroids in the diencephalon of older animals were frequently co-localized within areas of hemosiderosis and lipofuscinosis.

Neuronal lipofuscinosis was observed in 57 out of 71 brains (Figure 1c), while extracellular lipofuscin deposits were rare. Specifically, we observed lipofuscin in 15 group 1 animals, 11 group 2 animals, and all group 3 and group 4 animals. With H&E staining, lipofuscin appeared as golden–yellow, finely granular deposits within the soma, staining positive for carbol fuchsin long acid-fast stain (Figure 1c, inset). Lipofuscin was widely distributed throughout neurons of the cerebrum, brain stem, and cerebellar Purkinje cells. Lipofuscinosis was both age related and age progressive, with older monkeys (>10 years) more likely to display neuronal lipofuscin that increased in quantity and distribution with age progression. Specifically, a Kruskal–Wallis test showed that there was a significant difference of mean lipofuscin scores ($H = 30.33$, $p < .0001$); post hoc Dunn's multiple comparisons test found that the oldest group was significantly higher than two youngest groups (3–6 years old group, $p = .0001$; 7–9 years old group, $p < .0001$), and that group 3 score was significantly higher than group 2 ($p = .0066$). Group 1 was not significantly different from group 2 ($p > .9999$) and group 3 ($p = .541$), and group 3 was not significantly

TABLE 1 Main histopathological findings in the brains of 71 green monkeys.

Histopathologic finding	Description (H&E)	Intracellular or extracellular	Special stain	Commonly affected neuroanatomic sites	Animals affected per group			
					1 (n = 20)	2 (n = 20)	3 (n = 20)	4 (n = 11)
Hemosiderin	Iron-based yellow–brown pigment	Extracellular, intracellular (macrophages)	Perl's Prussian Blue	Thalamus, hypothalamus, globus pallidus	0 (0%)	1 (5%)	5 (25%)	9 (82%)
Spheroids	Round–ovoid, homogenous eosinophilic masses	Intracellular (axons)	N/A	Gracile nucleus, cuneate nucleus, hypothalamus, thalamus	5 (25%)	7 (35%)	9 (45%)	11 (100%)
Lipofuscin	Gray–yellow pigment	Intracellular (neuron bodies)	Carbol fuschin long acid-fast	Thalamus, pontine nucleus, olivary nucleus, FC GM, reticular formation, periaqueductal gray, limbic system	15 (75%)	11 (55%)	20 (100%)	11 (100%)
White matter vacuolation	Round, well-delineated clear spaces	Extracellular	N/A	Corona radiata, internal and external capsule, optic tract, corpus callosum, medulla oblongata (pons, obex), cerebellar medulla	20 (100%)	20 (100%)	20 (100%)	11 (100%)
Neuropil vacuolation	Round, well-delineated clear spaces	Extracellular	N/A	Cerebrum, cerebellum	20 (100%)	20 (100%)	20 (100%)	11 (100%)
Neuromelanin	Brown–black pigment	Intracellular (dopaminergic neuron bodies)	Fontana Masson	Hypothalamus, ventral tegmental area, substantia nigra	6 (30%)	3 (15%)	13 (65%)	11 (100%)
Reactive astrocytosis	Eccentric nuclei, swollen glassy pale eosinophilic cytoplasm	Cellular (astrocytes)	GFAP	Corona radiata, internal and external capsule; perivascular	0 (0%)	0 (0%)	3 (15%)	4 (36%)
Vascular mineralization	Basophilic, granular to crystalline	Intracellular (endothelial cells)	Von Kossa	Thalamus, globus pallidus	0 (0%)	1 (5%)	4 (20%)	2 (18%)
Melanin	Brown, granular pigment	Intracellular (melanocytes)	Fontana Masson	Meninges	16 (80%)	13 (65%)	14 (70%)	5 (45%)
Perivascular ceroid	Golden–yellow, finely granular	Intracellular (macrophages)	Carbol fuschin long acid-fast	Forebrain	20 (100%)	20 (100%)	20 (100%)	11 (100%)

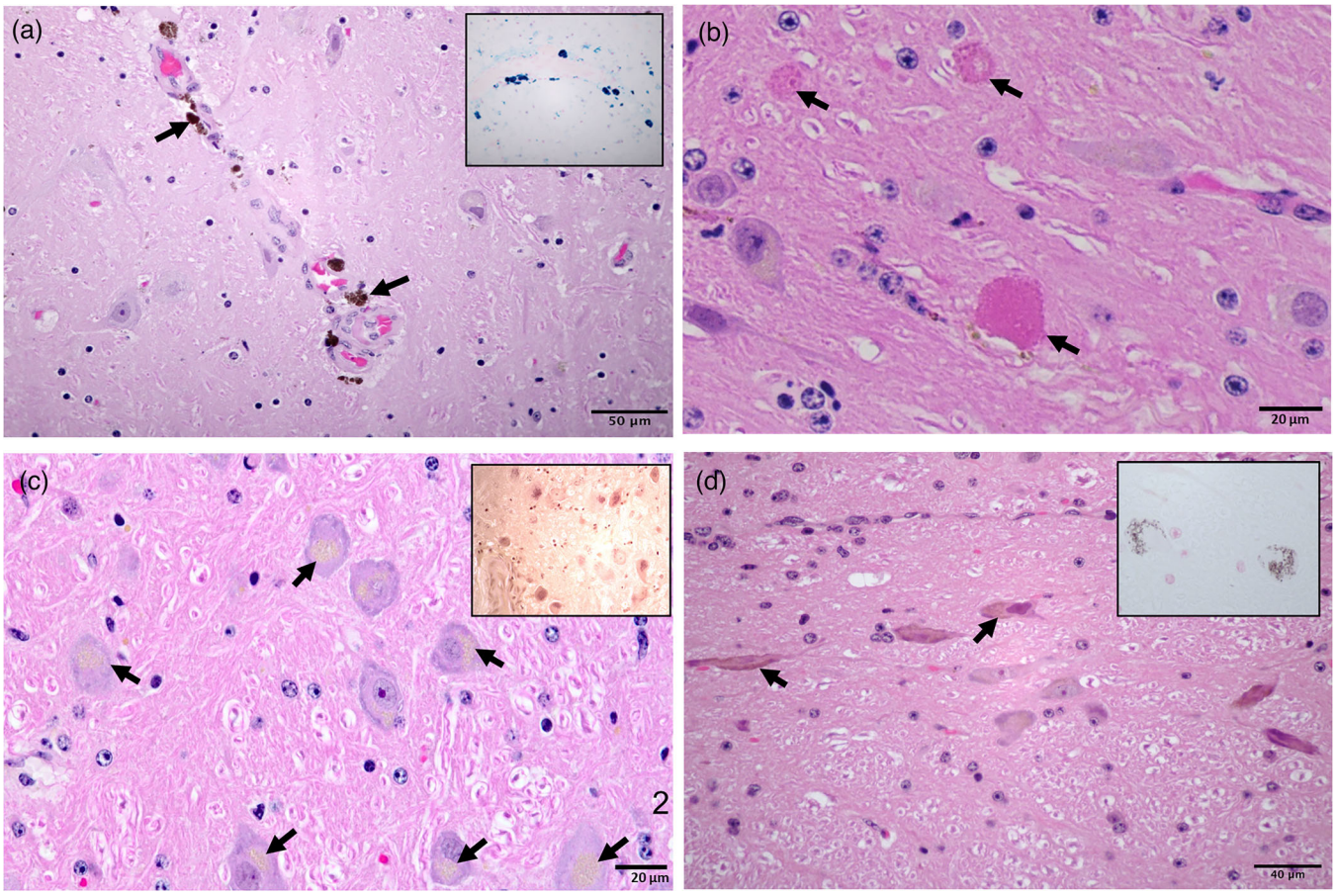

FIGURE 1 (a) Brain: thalamus; ~24-year-old AGM (No. 117). Perivascular hemosiderin deposits (arrows)—H&E, 40×; inset: Perl's Prussian blue (PPB) stain confirming the presence of iron in perivascular deposits, 40×. (b) Brain: thalamus; ~25-year-old AGM (No. 113). Spheroids (arrows)—H&E, 40×. (c) Brain: thalamus; ~25-year-old AGM (111). Intraneuronal lipofuscin (arrows)—H&E, 60×; inset: carbol fuchsin long acid-fast stain for ceroid and lipofuscin. (d) Brain: substantia nigra; ~25-year-old AGM (111). Intraneuronal neuromelanin (arrows)—H&E, 60×; inset: Fontana Masson stain confirming presence of neuromelanin.

different from group 4 ($p = .2155$) (Figure 4b). Neuromelanin was observed in 33 out of 71 animals in regions containing dopaminergic neurons, including the hypothalamus, ventral tegmental area, and substantia nigra (Figure 1d). This finding was also significantly age related ($p < .0001$); specifically, we observed neuromelanin in six group 1 animals, three group 2 animals, 13 group 3 animals, and all animals in group 4.

Round, well-delineated clear spaces, interpreted as WM vacuolation, were observed in multiple brain regions in all monkeys (71/71). WM vacuoles varied in size (5–40 μm) and frequency and were seen in the cerebrum, brainstem, and cerebellum (Figure 2a,b). The prevalence of WM vacuolation was not age related as it was seen in all monkeys independent of age. However, the number of vacuoles was age progressive, as the intensity of vacuolation per anatomical region increased significantly with increasing age. Kruskal–Wallis test showed that there was a significant difference of mean WM vacuolation scores ($H = 25.65$, $p < .0001$); post hoc Dunn's multiple comparisons test found that group 4 was significantly higher than group 1 ($p = .0001$), group 2 ($p < .0001$), and group 3 ($p = .0404$). Group 1 was not significantly different from group 2 ($p > .9999$) and group 3 ($p = .3719$), and group 2 was not significantly different from group 3 ($p = .1309$) (Figure 4b). Some WM areas, including the optic tract and corpus callosum, were consistently more vacuolated than surrounding WM regions, and vacuoles were observed in the optic tract of all brains.

Neuropil vacuolation was also observed in all monkeys (71/71). As within the WM, vacuoles varied in size and frequency (10–30 μm), and were found throughout the cerebrum, brainstem, and cerebellum. Comparable to WM vacuolation, neuropil vacuolation was age progressive, as the intensity of neuropil vacuolation per section increased significantly as age increased. Specifically, Kruskal–Wallis test showed that there was a significant difference of mean neuropil vacuolation scores ($H = 24.38$, $p < .0001$); post hoc Dunn's multiple comparisons test found that group 4 score was significantly higher than group 1 ($p = .0001$) and group 2 ($p < .0001$). Group 1 was not significantly different from group 2 ($p > .9999$) and group 3 ($p = .1813$), group 2 was not significantly different than group 3 ($p = .1309$), and group 3 was not significantly different from group 4 ($p = .2155$) (Figure 4b).

Eight of the monkeys displayed gliosis within WM and neuropil of the prefrontal and frontal cortices and globus pallidus. Three aged animals demonstrated glial nodules that were characterized by pallor and

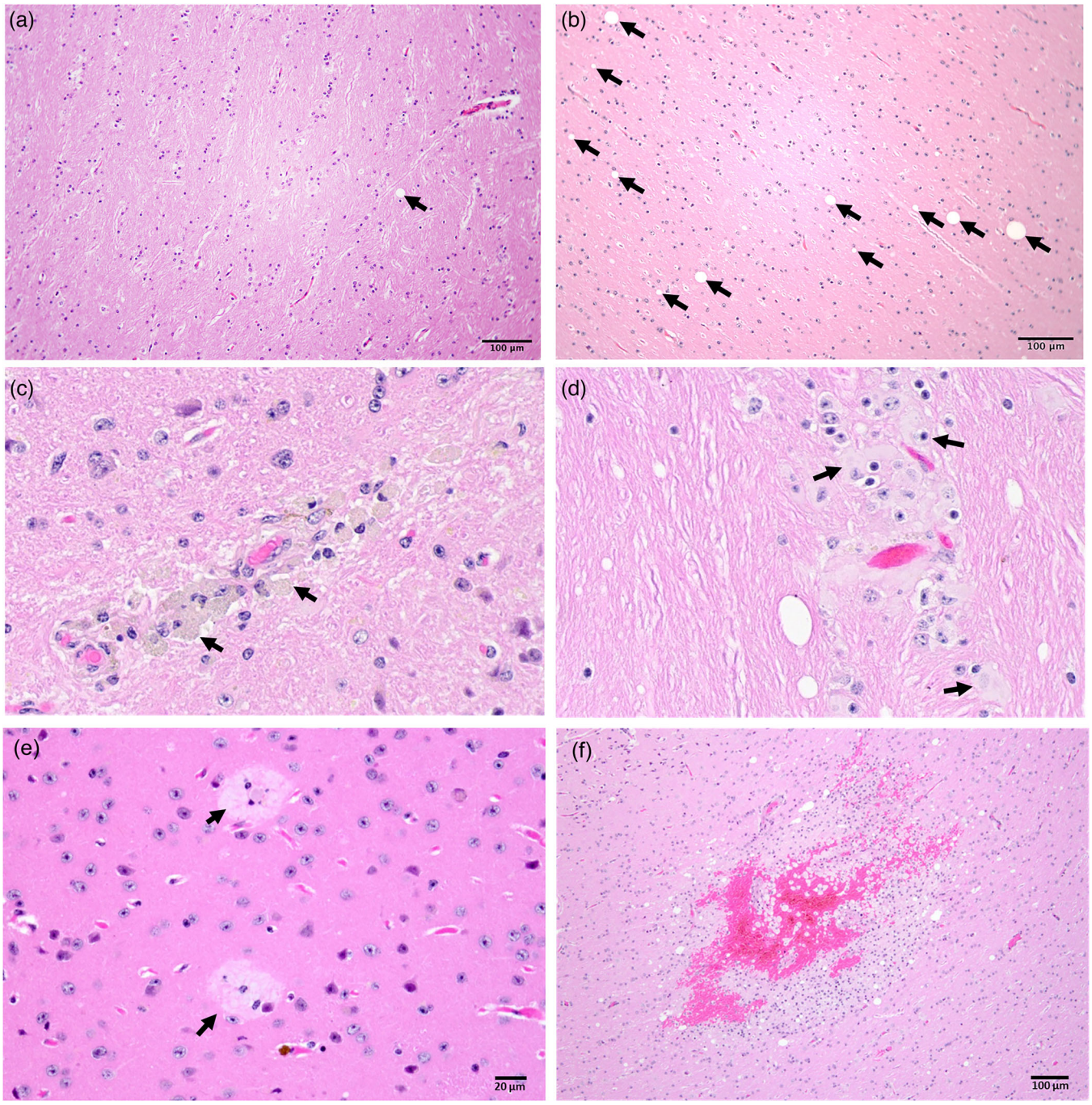

FIGURE 2 (a) Brain: internal capsule; 10- to 12-year-old AGM (No. 105). Minimal white matter vacuolation, equivalent to grade of 1 (arrows)—H&E, 20×. (b) Brain: internal capsule; ~25-year-old AGM (No. 113). Increased white matter vacuolation, equivalent to grade of 3 (arrows); additional smaller vacuoles are observed in the background—H&E, 20×. (c) Brain: prefrontal cortex white matter; ~25-year-old AGM (No. 111). Generalized gliosis (arrows) surrounding a focal area of perivascular gliosis with gitter cells containing yellow–brown finely granular intracytoplasmic debris (arrowhead and inset)—H&E, 20×. (d) Brain: frontal cortex, corona radiata; ~26-year-old AGM (No. 118). Perivascular gemistocytic astrocytosis—H&E, 40×. (e) Brain: frontal cortex; ~25-year-old AGM (No. 111). Round homogenous pale eosinophilic accumulations interpreted as Aβ plaques (arrows)—H&E, 40×. (f) Brain: dorsal frontal cortex, white matter; ~25-year-old AGM (No. 111). Focal region of liquefactive necrosis, hemorrhage, and gliosis—H&E, 10×.

spongiform change. Clusters of gitter cells containing yellow–brown finely granular intracytoplasmic pigment were seen within foci of gliosis, often located around small blood vessels (Figure 2c). Reactive astrocytes, characterized by eccentric nuclei and swollen glassy pale-eosinophilic cytoplasm, were diffusely scattered within forebrain WM tracts and rarely around blood vessels; this latter finding was recorded as perivascular gemistocytic astrocytosis (Figure 2d). Although some of this glial activity was immunopositive with GFAP, some was not; conversely, foci of GFAP immunopositivity did not always correspond with foci of gliosis observed with H&E. Reactive astrocytosis was most

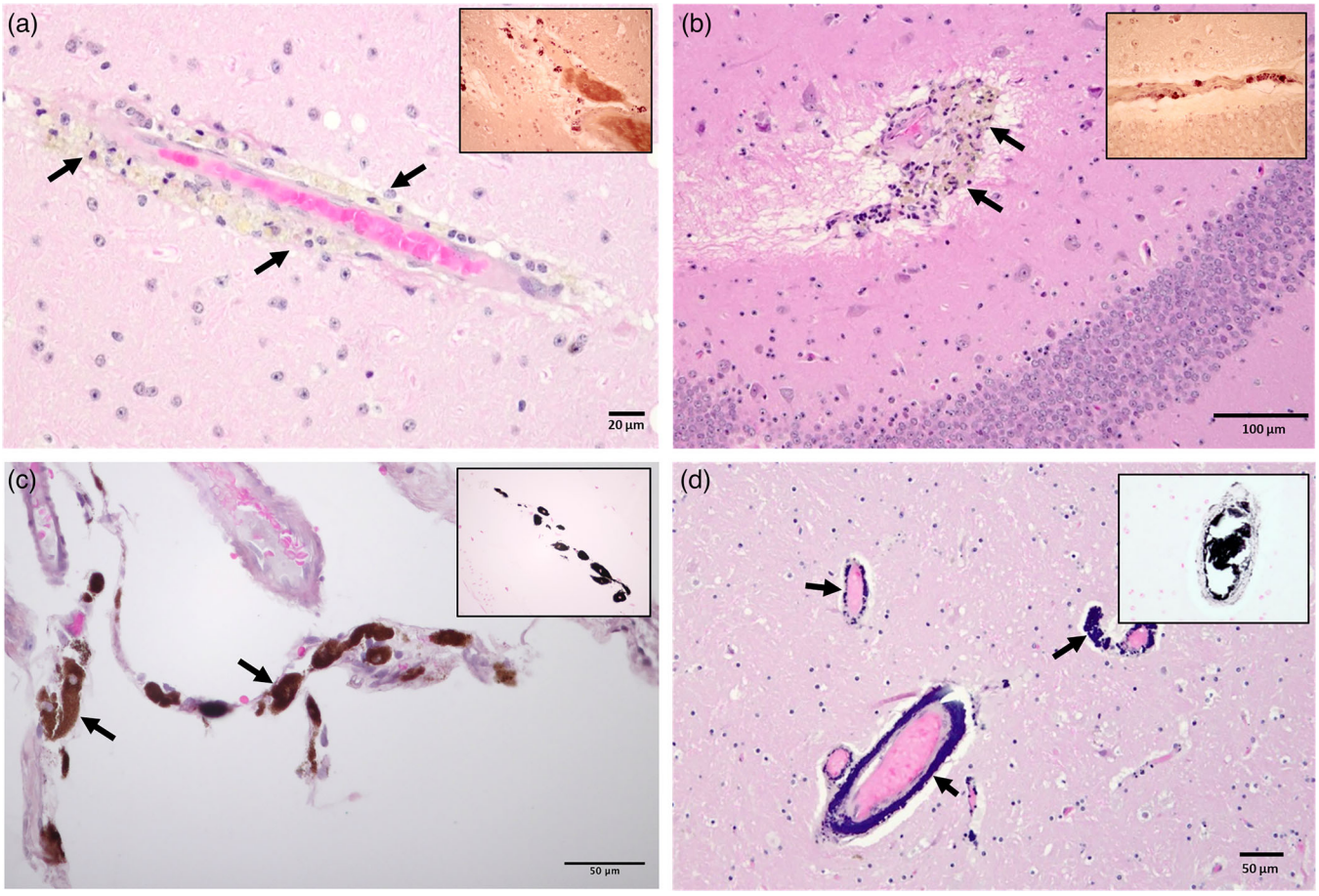

FIGURE 3 (a) Brain: frontal cortex; 7- to 9-year-old AGM (No. 99). Ceroid-laden macrophages in perivascular space (arrows)—H&E, 40×; inset: carbol fuchsin long acid-fast stain for ceroid and lipofuscin. (b) Brain: hippocampus; ~25-year-old AGM (No. 111). Ceroid-laden macrophages in perivascular space (arrows)—H&E, 20×; inset: carbol fuchsin long acid-fast stain for ceroid and lipofuscin. (c) Brain: meninges, frontal cortex; 10- to 14-year-old AGM (No. 62). Meningeal melanosis (arrows)—H&E, 40×; inset: Fontana Masson stain, confirming the presence of melanin. (d) Brain: thalamus; 10- to 14-year-old AGM (No. 65). Intramural vascular mineralization (arrows)—H&E, 20×; inset: Von Kossa stain confirming the presence of intramural calcification.

obvious in the three aged monkeys that died from *P. multocida* infections; however, similar astrocytosis was observed in four other monkeys that were euthanized and had no recent history of illness. Astrocytosis was only observed in monkeys over the age of 10 and increased significantly in incidence in older monkeys supporting an age-related characteristic ($p = .0034$). Mild lymphocytic perivascular cuffing was observed in FC WM of two monkeys, both 10–15 years old; in several aged monkeys, oligodendrocytes were observed clustering around blood vessels.

3.2 | Non-age-related histopathology

Ceroid pigment-laden macrophages were a non-age-related finding present in the perivascular space of all brains (71/71) (Figure 3a,b). Ceroid appeared golden–yellow and finely granular on H&E, staining positive with carbol fuchsin long acid-fast stain and negative with Perl's Prussian blue iron stain. While most deposits were small, occasional vessels had significant burdens of ceroid-containing macrophages that expanded the perivascular space. This pigment was associated with venules, capillaries, and arterioles in WM and neuropil of the forebrain, and rarely in the pons and medulla oblongata.

Melanosis was a common non-age-related finding, observed in 48 out of 71 animals ($p = .2364$) (Figure 3c); specifically, we observed melanin in 16 group 1 animals, 13 group 2 animals, 14 group 3 animals, and five group 4 animals. Melanin was predominantly found embedded in meninges, with occasional presence in the perivascular space of superficial blood vessels. Melanin appeared brown and granular with H&E staining and positive for Fontana Masson. Melanin was not observed during gross examination of the AGM meninges.

Vascular mineralization, primarily affecting arterioles and venules up to approximately 100 μm in diameter, was observed in the thalamus and globus pallidus of seven out of 71 animals (Figure 3d). With H&E staining, calcium deposits appeared deep purple and stained positivewith Von Kossa. Mineral deposits ranged from small globular accumulations in the tunica externa and tunica media to total permeation of the vessel wall. Mineralized vessels were commonly found in groups ranging from three to 50 vessels. While statistically the

presence of mineral did not appear to be age related ($p = .1171$), no mineral deposits were observed in the youngest group and all but one affected monkey was estimated to be over the age of 10 years; specifically, vascular mineralization was observed in one group 2 animal, four group 3 animals, and two group 4 animals.

A few incidental lesions were observed in the brain of older monkeys. On the dorsal surface of the left FC of a middle-aged monkey (estimated 13–15 years), surrounded by an area of gliosis, there was a cavitating pocket of liquefactive necrosis containing abundant gemistocytes, spheroids, hemosiderin, and foci of calcification. The cause for this focal region of pathology in this apparently clinically normal monkey is undetermined; however, hypoxic, ischemic, or toxic injury is suspected. In another aged monkey (estimated to be 25 years old), a focal area of hemorrhage, gliosis, liquefactive necrosis, spongiform change, and gitter cell accumulation was detected along WM tracts of the dorsal FC, which may represent a recent, small ischemic event (Figure 2f). Perivascular glial nodules containing clusters of gitter cells filled with yellow–brown finely granular intracytoplasmic pigment were observed in the lateral geniculate nucleus (LGN) of an aged (estimated 25 years old) monkey with phthisis bulbi of the right eye. The LGN, located at the junction between the thalamus and the optic nerve, acts as a relay center coordinating visual signaling from the retina to the thalamus. It is likely that the observed glial activity represents sequelae to the ocular damage. Reported findings in the LGN of NHPs after optic nerve transection include metabolic changes, astrocyte and microglial activation, and neuronal loss (Lam et al., 2009).

3.3 | AD-related pathology

On examination of H&E-stained slides from all 71 animals, roughly round homogenous pale eosinophilic accumulations, measuring 20–80 μm in diameter, interpreted as part of Aβ plaques, were observed in the cortical neuropil of the frontal and temporal lobes of 10 of these animals (Figure 2e). Nine of the monkeys were in group 4, only one was in group 3, and none was in groups 1 and 2 (Table 2). These plaques were confirmed by IHC to be 4G8-ir Aβ plaques. By IHC, Aβ plaques were roughly round and had an average diameter of 70 μm, with a diameter range of approximately 20–185 μm (Figure 5a,b). Some plaques were very dense and contained a central core of immunostaining, while others were less defined, more spread out, and granular. The observation of plaques was clearly age related, as nine of the 10 monkeys with plaques were >15 years old in group 4. The younger monkey with Aβ plaques belonged to group 3; none of the tested monkeys below the age of 10 showed detectable Aβ plaques (Table 2). Aβ plaques were quantified and were found to be age related, as a one-way ANOVA revealed that there was a statistically significant difference in the number of Aβ plaques observed between at least two groups ($4.164\ (3, 27) = 5.050$, $p = .0066$). Tukey's HSD test for multiple comparisons found that the mean number of Aβ plaques was significantly different between the oldest group when compared to each of the younger groups (groups 1 and 4 [$p = .0330$, 95% confidence interval, CI: −211.4, −6.978], groups 2 and 4 [$p = .0330$, 95% CI: −211.4, −6.978], groups 3 and 4 ($p = .0276$, 95% CI: −173.6, −7.987]). There was no statistically significant difference between the mean number of plaques observed in the three younger groups (groups 1 and 2 [$p > .9999$], groups 1 and 3 [$p > .9617$], groups 2 and 3 [$p = .9617$]) (Figure 9). Plaques were identified in all cortical layers of the PFC and TC of all 10 affected monkeys. Additionally, plaques were observed in all cortical layers of the FC of nine of these animals and in the CC of seven of them. Aβ plaques within the EC were found in one female verifiably older than 19 years (estimated to be 25 years old). Based on IHC of adjacent sections, increased GFAP expression profiles were highly suggestive of co-localization with most Aβ plaques in all 10 monkeys (Figure 6). In addition to the clearly defined amyloid plaques, scattered granular extracellular Aβ was occasionally detected within cortical neuropil (Figure 5a,c). Four additional monkeys, three in group 3 and one in group 4, exhibited these scattered extracellular Aβ deposits without detectable amyloid plaque formation.

Prominent intramural vascular Aβ-positive profiles were found in nine out of 31 monkeys and increased significantly with age (Table 2). All but one animal with detectable Aβ plaques presented with Aβ deposition within vascular walls; intramural vascular Aβ deposits were not observed in any monkey lacking Aβ plaques. Eight of the nine affected monkeys were in group 4; the outlier, from group 3, was the same animal with demonstrable Aβ plaques. In these monkeys, the tunica media and tunica adventitia of parenchymal blood vessels in the affected cortex were often completely infiltrated by Aβ (Figure 5c). While blood vessels were primarily observed along the cortical surface, Aβ deposits were also found within the immediate perivascular neuropil in the all layers of the PFC, occasionally in the FC and TC, and rarely at the gray/white matter interface and subcortical WM tracts (Figure 5d). The neuropil immediately adjacent to Aβ-affected blood vessels occasionally had positive expression profiles for both 4G8 and GFAP.

When evaluating for evidence of tau pathology, bright-field examination revealed the presence of abnormal p-tau, a precursor to NFT formation, by CP13 (but not AT8) positive profiles in the FC and MTL of AGMs. These regions were specifically selected for evaluation because in the pathogenesis of AD, NFTs are first observed within neurons of the EC and hippocampus, and later extend to the amygdala and deep cerebrocortical layers of the temporal, frontal, and parietal lobes, a spatiotemporal progression that strongly correlates with the progression and severity of clinical signs in AD patients (Sanabria-Castro et al., 2017). However, no AGM brain evaluated presented frank NFTs at any age. CP13-ir appeared in the neuropil, fibers, and cells as a granular immunostain in young, middle-aged, and old AGMs. Interestingly, single, pairs, or groups (nest) of small CP13-ir cells resembling oligodendrocytes were found mainly in the WM of the FC and MTL in some of the monkeys. In general, most of the AGMs displaying p-tau in the MTL had some degree of CP13 immunostain in the FC and group 1 had the lowest number of animals showing p-tau-positive profiles (Table 2).

Specifically in the FC, CP13-ir profiles were found in one group 1 animal, five group 3 animals, and four group 4 animals. In the youngest AGM, CP13-positive cells and neuropil were observed in OC and CC

TABLE 2 Alzheimer's disease related findings in the brains of 31 green monkeys.

Group	1					2					3										4										Common locations (number of monkeys affected)	Age-related?
Animal ID	**29**	**46**	**48**	**49**	**88**	**32**	**38**	**57**	**74**	**79**	**41**	**58**	**59**	**82**	**105**	**106**	**107**	**108**	**114**	**115**	**81**	**83**	**84**	**109**	**110**	**111**	**112**	**113**	**116**	**117**	**118**	
Age range	3–6 years					7–9 years					10–15 years										>15 years											
Aβ plaques (4G8)	–	–	–	–	–	–	–	–	–	–	–	✓	–	–	–	–	–	–	–	–	✓	–	–	✓	✓	✓	✓	✓	✓	✓	✓	Prefrontal cortex (10/10) Frontal cortex (9/10) Cingulate cortex (7/10) Temporal cortex (10/10) Entorhinal cortex (1/10)	Yes $p = .0066$
Aβ plaques observed by H&E	–	–	–	–	–	–	–	–	–	–	–	✓	–	–	–	–	–	–	–	–	✓	–	–	✓	✓	✓	✓	✓	✓	✓	✓	Frontal cortex (10/10) Temporal cortex (10/10)	Yes $p < .0001$
Scattered extracellular Aβ (4G8)	–	–	–	–	–	–	–	–	–	–	–	✓	–	–	✓	–	–	–	✓	✓	✓	✓	–	✓	✓	✓	✓	✓	✓	✓	✓	Prefrontal cortex (14/14) Frontal cortex (14/14) Temporal cortex (12/14) Cingulate cortex (11/14) Entorhinal cortex (1/14)	Yes $p = .0005$
Aβ CAA (4G8)	–	–	–	–	–	–	–	–	–	–	–	✓	–	–	–	–	–	–	–	–	✓	–	–	✓	✓	✓	–	✓	✓	✓	✓	Cortical surface (9/9) Prefrontal cortex (9/9) Frontal cortex (5/9) Temporal cortex (5/9) Subcortical WM tracts (5/9) GM/WM interface (4/9)	Yes $p = .0011$
GFAP-ir with plaques	–	–	–	–	–	–	–	–	–	–	–	✓	–	–	–	–	–	–	–	–	✓	–	–	✓	✓	✓	✓	✓	✓	✓	✓	NA	NA
Phosphorylated tau (CP13)	✓	✓	–	–	–	–	–	–	–	–	–	–	–	–	✓	✓	✓	✓	✓	✓	–	–	–	✓	✓	✓	✓	✓	–	–	✓	Cingulate cortex (10/10) Orbital cortex (9/10) Prefrontal cortex (8/10) Entorhinal cortex (7/12) Subiculum (6/12) Hippocampus—CA1/CA3 (12/12) Hippocampus–dentate gyrus (3/12)	No $p = .235$ (FC) No $p = .203$ (MTL)

Note: For each finding, the proportion of affected monkeys, the main anatomical regions affected, and statistical significance of findings are listed. No = not significantly related to age; yes = significantly related to age. NA = not analyzed. Organized by four evaluated groups, the individual animal results for AD-related pathology are presented. – = listed pathology not observed in this animal; ✓ = listed pathology observed in this animal.

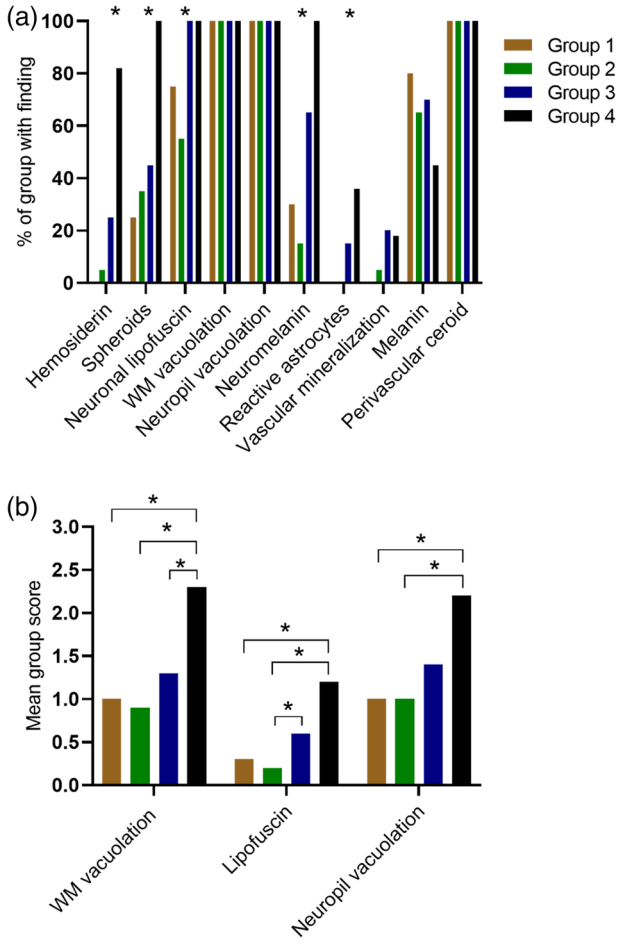

FIGURE 4 Histopathology findings in the brains of 71 green monkeys. (a) Percent of animals per group that demonstrated a given finding, reported by group; *p* values were calculated using Chi-square: $^*p < .05$. (b) Mean group scores for white matter vacuolation, neuronal lipofuscin, and neuropil vacuolation; *p* values were calculated using Kruskal–Wallis test with post hoc Dunn's multiple comparison test: $^*p < .05$.

layers I–III (Figure 7a,b), while in middle-aged and old AGMs CP13 profiles were also found in the PFC (Figure 7c–h). In four of five middle-aged AGMs, CP13-ir neurons and fibers were observed in layers II, III, and V of the CC (Figure 7c), and CP13 immunostaining in the neuropil of the OC, FC, and CC layers was consistently reduced from the supragranular to the infragranular layers (Figure 7c,d,f,g). In addition, one of the monkeys exhibited numerous CP13-ir oligodendrocyte-like cells between the white and gray matter transition areas in the OC, CC, and PC. By contrast, the fifth monkey displayed mainly CP13 stain in the neuropil, but not in cells, of PC, CC, and OC layers I and II. In the old AGMs FC, CP13-ir profiles displayed stronger and more extended distribution compared to the youngest and middle-aged monkeys (Figure 7a–e). Among the four aged monkeys containing p-tau, one exhibited the greatest amount of CP13-ir in the neuropil, neurons, and fibers of the PFC, CC, and OC (Figure 7f–h). The other three aged AGMs displayed lighter staining in the neuropil of the CC and PC compared to the OC. While pale CP13-ir neurons and fibers were commonly seen in the cingulate layers II and III in these monkeys, the PC and OC exhibited strong CP13-ir oligodendrocyte-like cells in the white and gray matter.

In the MTL, CP13 immunoreactivity was detected in two group 1 animals, five group 3 animals, and six group 4 animals. The youngest monkeys exhibited CP13 immunoreactivity in the neuropil and cells of EC layers I and II, subicular and hippocampal cornu ammonis (CA) 1 field cells as well as in bundles of fibers in the hippocampal CA3 field (Figure 8a–c). Four of the five middle-aged monkeys exhibited some degree of staining either in the dentate gyrus granule cells, hilus, the CA3 fiber bundle, hippocampal CA1 neurons, subicular cells, or the EC (Figure 8d–j). In addition, CP13-ir oligodendrocyte-like cells were seen in the subiculum and EC WM in one monkey (Figure 8h). The fifth monkey displayed only a pale CP13 stain in the CA3 fiber bundle. Among the six p-tau-positive monkeys in the oldest AGM group (Figure 8k–v), one exhibited the greatest extent of CP13-ir profiles in the hippocampal CA fields, dentate gyrus granule cell layer, hilus, subiculum, and EC (Figure 8k–p). Three monkeys exhibited CP13-ir neuropil, cells, and fibers in the EC, subiculum, and CA3 field (Figure 8q–v), while only two displayed pale CP13-ir tract stains in the hippocampal CA3 field. In addition, CP13-ir oligodendrocyte-like cells were also observed in the subiculum and EC in some of these monkeys (Figure 8r,s).

4 | DISCUSSION

Histopathological changes were observed in all 71 brains examined; however, none of these AGMs showed neurological signs at the time of death. Therefore, the histologic findings in this study are thought to represent age- and non-age-related background pathology within the brain of AGMs without clinical evidence of neurological disease. Here, we found that hemosiderin deposition, spheroids, neuronal lipofuscinosis, neuromelanosis, WM and neuropil vacuolation, glial nodules, and reactive astrocytosis were age-dependent histopathological findings, while perivascular ceroid deposition, meningeal melanosis, and vascular mineralization were non-age-related findings. Occasionally observed were neuropathologic findings, interpreted as incidental, included lymphocytic perivascular cuffing, irregular oligodendrocyte formations, and focal liquefactive necrosis. The fact that the non-age-related changes were consistently observed in AGM brains across all ages suggests that such changes are not a manifestation of an underlying condition or disease process. Our findings were often consistent with background neuropathological findings reported in studies examining other NHP species as well as humans, horses, cattle, pigs, sheep, dogs, cats, and rodents (summarized with references in Table 3). Moreover, Aβ-plaque pathology was observed as early as 10–15 years of age in animals and exhibited an age-related accumulation and progression in AGM brain. The present study, using a combination of morphologic and molecular diagnostic techniques, provides a comprehensive assessment of background and AD-like pathology within the brain of the largest group of AGMs investigated to date. Our findings support the aged AGM as a natural model of Aβ pathology and cerebral amyloid angiopathy (CAA), validating previous reports of age-progressive

TABLE 3 Naturally occurring background neuropathology in humans and animal species.

Species/Lesion	Hemosiderin	Spheroids	Lipofuscin	Neuromelanin	Vacuolation or Myelin Damage	Gliosis or Astrocytosis	Ceroid	Vascular Mineralization	Meningeal Melanosis
Humans	✓[20]	AR[3,9,20]	AR[25]	AR[25,38,39]	AR[21]	AR[28]	AR[27]	AR[22,36]	✓[11]
AGM	AR	AR	AR	AR	AR	AR	✓	✓	✓
Macaques	AR[29]	AR[4,7,29]	AR[7,29]	AR[13,24]	AR[15,29]	AR[6,29]	AR[15]	✓[29,32]	–
Squirrel Monkeys	AR[14]	AR[7]	AR[7]	AR[38]	AR[14]	AR[14]	–	–	–
Mice & Rats	–	–	AR[38]	–[24]	–	–	–	✓[35,37]	✓[12]
Dogs	–	AR[2,31]	AR[2,31]	AR[38]	AR[38]	AR[2,32,38]	AR[38]	AR[8,38]	–
Cats	✓[23]	–	AR[38]	✓[24]	–	✓[33]	–	✓[23]	–
Cattle	-	✓[10]	AR[38]	–	✓[10,19]	AR[10]	–	AR[10,34]	✓[33]
Sheep	✓[30]	✓[16]	-	✓[24]	✓[30]	✓[38]	–	–	✓[8]
Horses	✓[17]	✓[1,17]	AR[17]	✓[24]	✓[17]	AR[5]	–	AR[17]	–
Pigs	–	✓[18]	AR[26]	–	✓[18]	–	–	–	–

Compilation of background neurohistopathological changes occurring naturally in a number of animal species, compared to those observed in this AGM study. AR= age-related change. ✓=non-age-related/not specified to be age related. (–) = not present or not described in the literature (to our knowledge). Macaque species included are cynomolgus and rhesus macaques.

1. Beech, 1984; 2. Borràs et al., 1999; 3. Brannon et al., 1967; 4. Bronson & Schoene, 1980; 5. Capucchio et al., 2010; 6. Chamanza et al., 2010; 7. Cork & Walker, 1993; 8. Fankhauser, 1968; 9. Fujisawa, 1967; 10. Gavier-Widen et al., 2001; 11. Goldgeier et al. 1984; 12. Gudjohnsen et al., 2015; 13. Herrero et al., 1993; 14. Heuer et al., 2017; 15. Hof et al., 2002; 16. Hooper, 1999; 17. Jahns, Callanan, McElroy, et al., 2006; 18. Jahns, Callanan, Sammin, et al., 2006; 19. Jeffrey, 1992; 20. Jellinger & Jirásek, 1971; 21. Liu et al., 2016; 22. Lowe et al., 1997; 23. Mandara et al., 2001; 24. Marsden, 1961; 25. Moreno-García et al., 2018; 26. Nanda & Getty, 1971; 27. Neltner et al., 2015; 28. Norden & Godbout, 2013; 29. Sasseville et al., 2012; 30. Sharpe, 2004; 31. Suzuki et al., 1979; 32. Wadsworth et al., 1995; 33. Wohlsein et al., 2012; 34. Xiao, 2016; 35. Yanai et al., 1994; 36. Yanai et al., 1993; 37. Yanai et al., 1987; 38. Youssef et al., 2016; 39. Zecca et al., 2001.

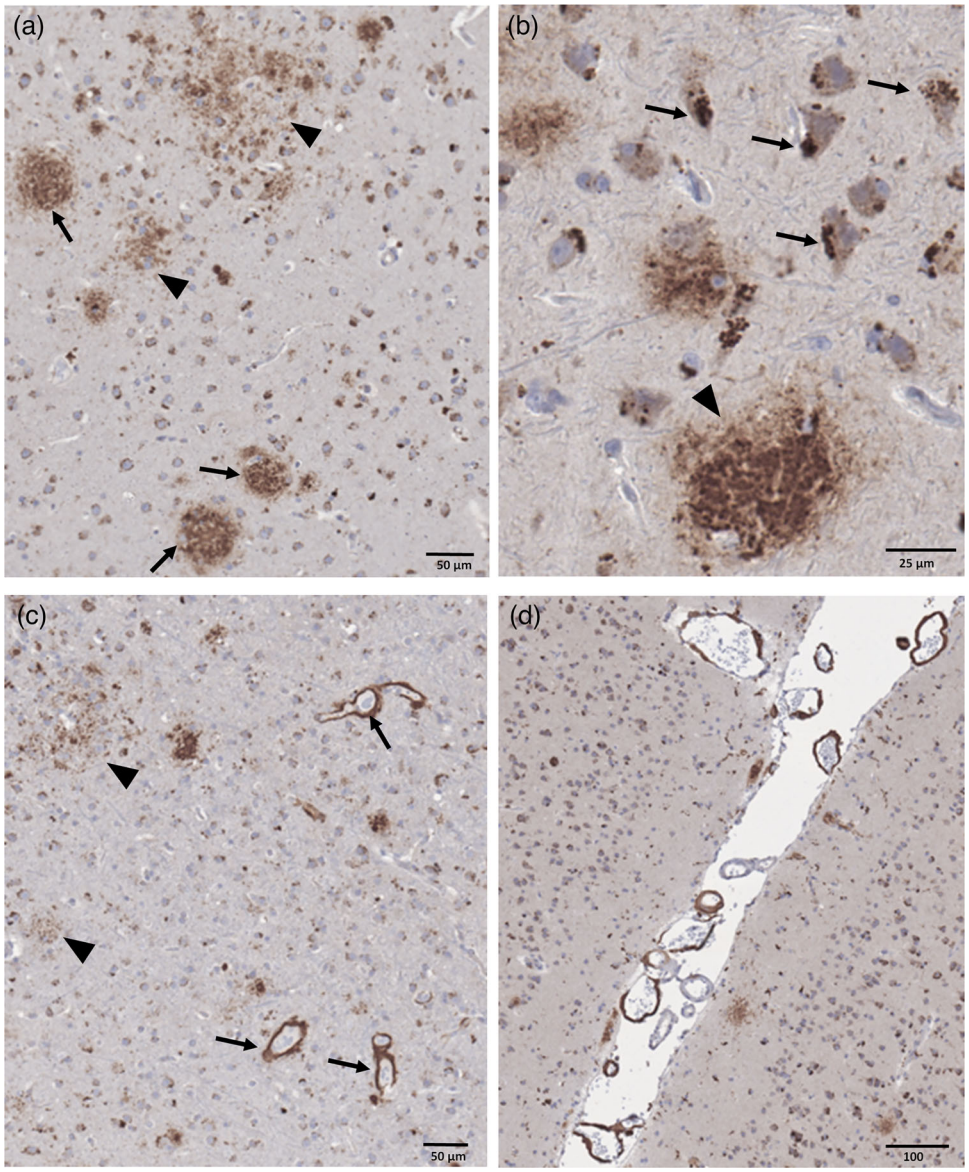

FIGURE 5 (a) Brain: temporal cortex; >18-year-old AGM (No. 109). Extracellular Aβ plaques (arrows); granular Aβ deposits (arrowheads). (b) Brain: entorhinal cortex; ~25-year-old AGM (No. 111). Extracellular Aβ plaque (arrowhead); intraneuronal Aβ immunoreactivity (arrows). (c) Brain: temporal cortex; ~24-year-old AGM (No. 117). Intramural vascular Aβ deposits (arrows); extracellular Aβ deposits (arrowheads). (d) Brain: prefrontal cortex; ~25-year-old AGM (No. 111). Meningeal blood vessel Aβ deposits (arrows).

cerebrocortical Aβ-ir amyloid plaques and vascular deposits associated with increased GFAP immunostaining, in addition to abnormal p-tau within the MTL and FC.

Perivascular and neuropil hemosiderin deposits were age-related changes in AGMs. These deposits showed an iron-based yellow–brown pigment derived from the breakdown of hemoglobin within areas of hemorrhage and frequently associated with lipofuscinosis, intramural vascular mineralization, gliosis, and spheroids. Perivascular hemosiderin deposits have also been reported in aged rhesus macaques and humans, and as an incidental finding in other animal species (Bronson & Schoene, 1980; Jahns, Callanan, McElroy, et al., 2006; Jellinger & Jirásek, 1971; Mandara et al., 2001; Sasseville et al., 2012; Sharpe, 2004). In aged humans, hemosiderin-laden macrophages in the perivascular space are indicative of prior microbleeds (Grinberg & Thal, 2010). The increased prevalence of hemosiderin deposits in aged AGMs may indicate an increased incidence of cerebral microhemorrhages, or alternatively may be evidence of a compromised blood–brain barrier in these aged NHPs with an extracranial source of hemosiderin. Hemosiderin-laden macrophages have been observed in several other organs in the AGM including, but not limited to, the lungs and kidneys (unpublished data; P. Bolfa, 2019, Ross University School of Veterinary Medicine). Many NHPs used in biomedical research, including our AGMs, commonly undergo femoral venipuncture for blood collection resulting in small regional hematomas, which could serve as a source of circulating hemosiderin in these animals as well (Wolf & White, 2012).

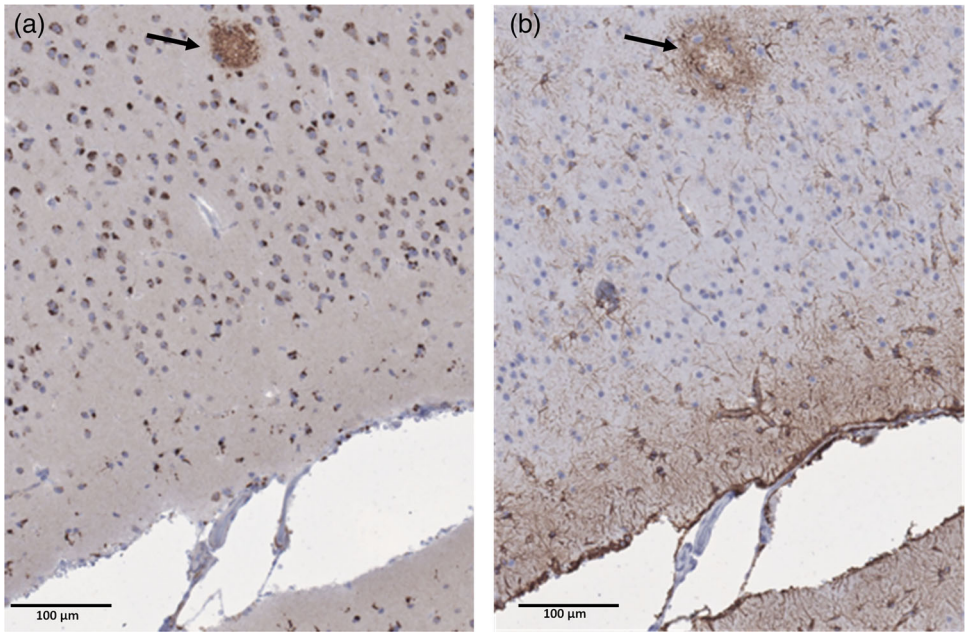

FIGURE 6 Brain: prefrontal cortex; ~25-year-old AGM (No. 112). (a) 4G8-ir Aβ plaques. (b) Likely co-localized GFAP expression.

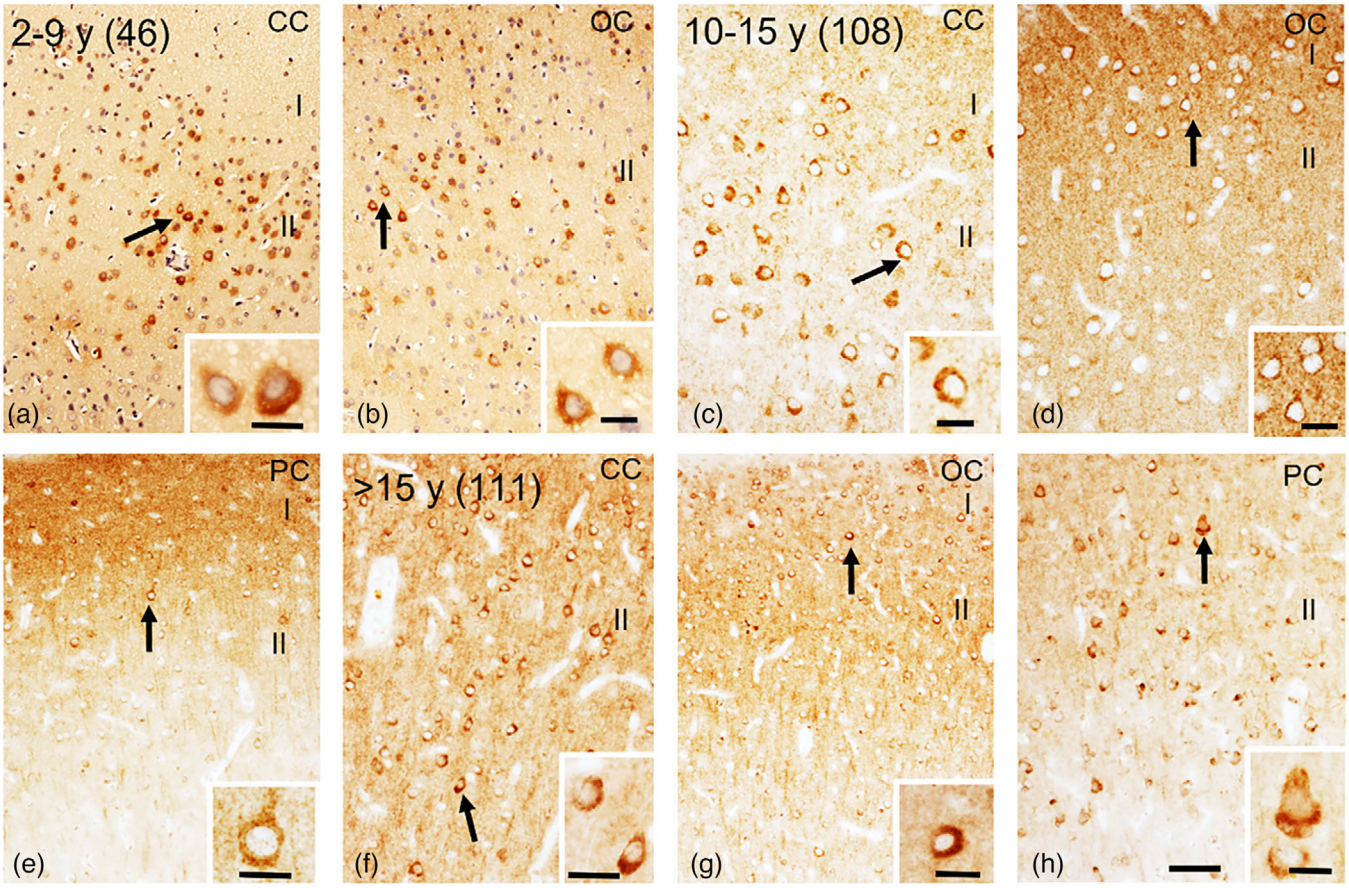

FIGURE 7 Frontal cortex images showing CP13-ir profiles in the cingulate (CC), orbital (OC), and prefrontal (PC) cortex in a young (A, B; No. 46), middle-aged (C–E; No. 115, 106), and old (F–H; No. 111) AGM. Insets in panels (a–d) and (e–h) show high-magnification images of CP13-positive cells indicated by arrows. Note that oldest AGM exhibited more CP13-ir profiles in the FC compared to the youngest and middle-aged monkeys. Tissue in panels (a) and (b) was counterstained with Mayer's hematoxylin. Scale bar: (h) 50 μm and applies to (a, b, e–g); (c, d) 25 μm; insets = 20 μm.

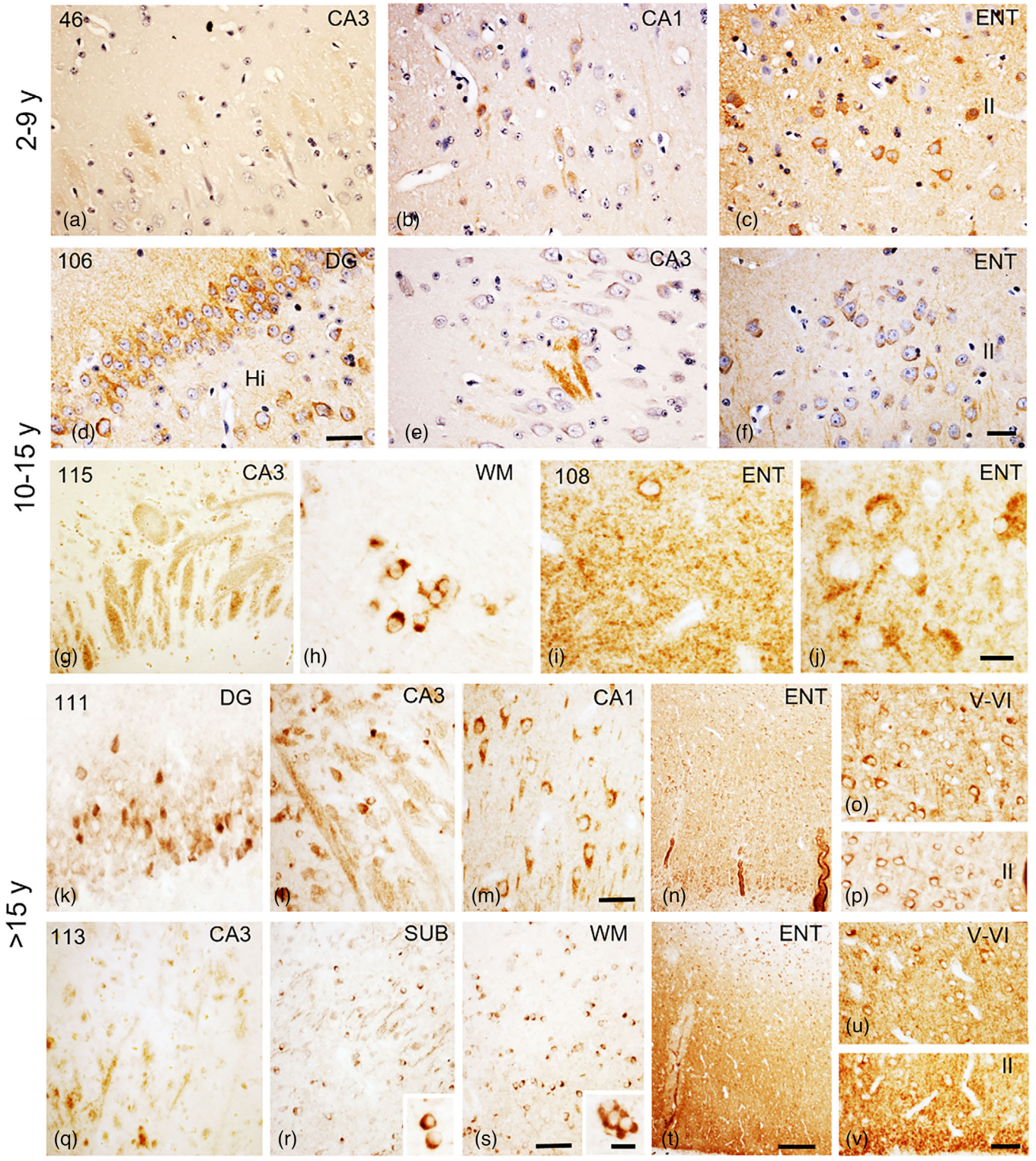

FIGURE 8 Images showing CP13-ir profiles in hippocampal CA1 and CA3 fields, dentate gyrus (DG) granule cell layer and hilus (Hi), subiculum (SUB), and entorhinal (ENT) gray (layers II and V–VI) and white matter (WM) in young (A–C; No. 46), middle-aged (D–J ; No. 106, 115), and old (K–V; No. 111, 113) AGMs. Insets in panels (r) and (s) show high-power images of CP13-ir oligodendrocytes-like cells in the subiculum and entorhinal cortex WM, respectively, in a monkey older than 15 years. Note many more CP13-ir profiles in the entorhinal cortex of the oldest (N–P and T–V) compared to young and middle-aged AGMs (c, f, i, and j) and the presence of CP13-ir oligodendrocytes-like cells in groups or nests in the entorhinal cortex WM (s). Bundles of CP13-ir fibers in hippocampal CA3 field were more notorious in the oldest and middle-aged (g, l, q) compared to the youngest (a) AGM. Tissues in panels (a–f) were counterstained with Mayer's hematoxylin. Scale bar: (f) 25 μm and applies to (a–c, e, g); (d) 25 μm; (j) 10 μm and applies to (h, i); (m) 20 μm and applies to (k, l); (s) 50 μm and applies to (q–s); (t) 100 μm and applies to (n); (v) 50 μm and applies to (o, p, u); inset in (s) = 10 μm and applies to inset in (r).

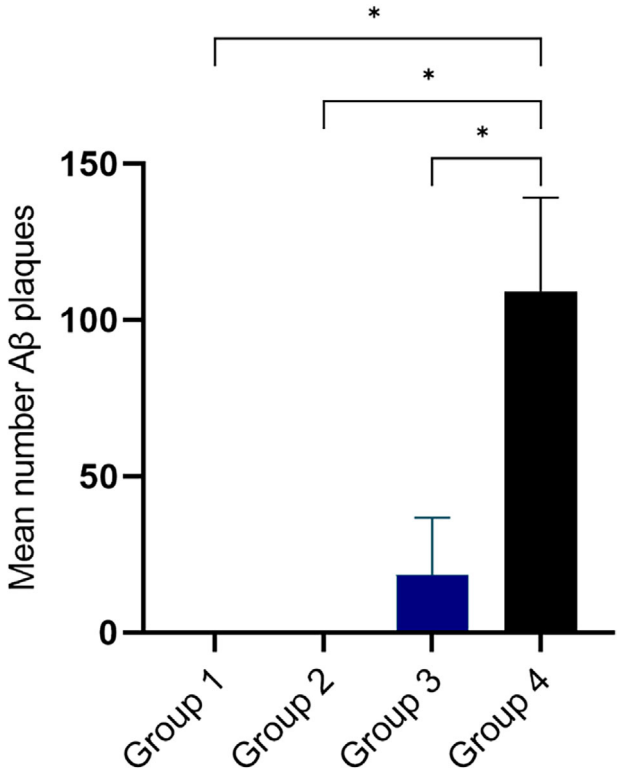

FIGURE 9 Mean number of total plaques, reported by age group; *p* values were calculated using one-way ANOVA with Tukey's HSD test for multiple comparisons: $^{*}p < .05$.

The finding of age-related spheroids, or axonal swellings, is consistent with what has been reported in a wide range of species (Beech, 1984; Borràs et al., 1999; Brannon et al., 1967; Gavier-Widen et al., 2001; Hooper, 1999; Jahns, Callanan, McElroy, et al., 2006; Jahns, Callanan, Sammin, et al., 2006; Jellinger & Jirásek, 1971; Newberne et al., 1960; Suzuki et al., 1979). The anatomical distribution of these spheroids in AGMs, including their preponderance within the gracile nucleus, globus pallidus, thalamus, and substantia nigra, was similar to the clinically normal aged rhesus and squirrel monkeys findings (Bronson & Schoene, 1980; Cork & Walker, 1993; Sasseville et al., 2012). The etiology of spheroids is multifactorial, though they are frequently connected with neuronal degeneration in cases of neuroaxonal dystrophy, trauma, hypoxia, lysosomal storage disorders, and vitamin deficiencies (Jahns, Callanan, McElroy, et al., 2006). These observations indicate that certain brain regions are susceptible to neurodegeneration with age in NHPs.

Our findings of age-related and age-progressive lipofuscin accumulations in the AGM are consistent with patterns observed in humans, other NHPs, and many other animal species (Borràs et al., 1999; Cork & Walker, 1993; Jahns, Callanan, McElroy, et al., 2006; Kikuchi, 1928; Nanda & Getty, 1971; Sasseville et al., 2012; Suzuki et al., 1979). Lipofuscin, a "wear and tear pigment" derived from lysosomal catabolism of lipids, metals, and proteins, is a common finding with aging (Cork & Walker, 1993). Lipofuscin has traditionally been considered an innocuous consequence of the aging process; however, lipofuscin is known to alter neuron cytoskeletal function and cellular metabolism, contributing to free radical formation and oxidative stress on the cell, and has been associated with neuron loss and neuroinflammation. In recent years, lipofuscin has been further investigated as having an active role in neurodegenerative diseases including AD, Parkinson's disease, and macular degeneration. In AD, lipofuscin is found to co-localize with amyloid plaques, and it is proposed that the release of lipofuscin into extracellular neuropil following neuron death may contribute to plaque formation and neurodegeneration (Moreno-García et al., 2018). In our study, high prevalence and intensity of neuronal lipofuscinosis was correlated with extensive Aβ plaque formation; however, we did not identify extracellular lipofuscin within or around these plaques, perhaps suggesting the absence of associated neuronal death.

Neuromelanin, a dark catecholaminergic metabolite commonly found within neurons of the human dopaminergic system, was observed at higher frequencies within neurons of the hypothalamus, ventral tegmental area, and substantia nigra in older animals, consistent with previous reports in NHPs and other nonprimate species (Herrero et al., 1993; Marsden, 1961; Youssef et al., 2016). In humans, neuromelanin concentration also increases with age, and neuromelanin-containing neurons have been of particular interest in Parkinson's disease research. Neuromelanin levels in the substantia nigra of Parkinson's patients are significantly lower than that in age-matched controls (Zecca et al., 2001). While the exact role of neuromelanin in the pathogenesis of Parkinson's disease remains unknown, the accumulation of this pigment in dopaminergic cells, particularly in the substantia nigra, has been associated with deficits in cellular function and neuronal cell death (Stepień et al., 2007).

WM vacuolation, and to a lesser extent neuropil vacuolation, was observed in all 71 AGM brains; however, the intensity of the vacuolation increased significantly with age. These changes may represent vacuolar changes of neuronal cell processes within the neuropil and/or vesiculation of myelin sheaths (Wohlsein et al., 2012). Vacuoles varied in size and frequency, and were seen throughout the brain, with increased vacuole density in the optic tract and corpus callosum. Age-related vacuolation and myelin sheath pathology have been described in the rhesus macaque, with similar distributions, including in the primary visual cortex and optic tract, anterior commissure, corpus callosum, inferior colliculus, cochlear and olivary nuclei, substantia nigra, and the cerebellum (Hof et al., 2002; Sasseville et al., 2012). The occasional perivascular cuffing, as well as the increased association of oligodendrocytes with small blood vessels observed in some aged AGM brains, is also a consistent finding described in the aged rhesus macaque (Hof et al., 2002), and may be a response to, or the result of, myelin sheath and neuropil alterations leading to the observed vacuolation. Additionally, vacuolar degeneration in clinically normal animals is reported in several other animal species (Gavier-Widen et al., 2001; Jahns, Callanan, McElroy, et al., 2006; Jahns, Callanan, Sammin, et al., 2006; Sharpe, 2004). These data suggest that vacuolation is an indicator of myelin sheath/axonal alterations in aged animals that may lead to neurodegeneration.

While differential diagnoses for vacuolar changes include degenerative diseases, myelin edema, spongiform myelinopathies, toxic

disorders, metabolic derangements, and renal or hepatic disorders (Jahns, Callanan, McElroy, et al., 2006; Wohlsein et al., 2012), vacuolation can also be an artifact created during tissue preparation and processing for microscopic assessment. This is particularly common in frozen or suboptimally fixed tissue, autolyzed tissue containing saprophytic gas-producing bacteria, or tissue that has undergone prolonged exposure to 70% alcohol (Jahns, Callanan, McElroy, et al., 2006; Wohlsein et al., 2012). In our study, the possibility of artifactual vacuolation of the WM or neuropil was unlikely, as in most monkeys (67/71), the brain was collected immediately after euthanasia, decreasing the risk of tissue postmortem autolysis, and postfixed in adequate volumes of 4% paraformaldehyde for at least 1 week. The four brains with delayed collection were interpreted with caution, although the vacuolation observed was similar in distribution and frequency to that present in the brains of euthanized animals from the same group. None of the brains in this study were frozen or exposed to 70% alcohol. We propose that, like earlier discussed reports in the aged rhesus macaque (Hof et al., 2002; Sasseville et al., 2012), some vacuolation may be the result of degenerative changes in myelin sheaths, representing a background finding that becomes more prominent and significant as AGMs age. However, the high level of vacuolation consistently observed in the corpus callosum and the optic tract of most monkeys, which was not age related or accompanied by cognitive or visual deficits, likely represents an increased susceptibility to artifactual vacuolation in these particular regions of the brain.

The etiology for the gliosis and reactive astrocytosis observed in the aged monkeys is not clear, as gliosis is a nonspecific finding described in inflammatory, infectious, neoplastic, and neurodegenerative diseases (Youssef et al., 2016). Gliosis and/or reactive astrocytosis of unspecified origin has been reported in aged humans, NHPs, and other animal species (Borràs et al., 1999; Capucchio et al., 2010; Chamanza et al., 2010; Gavier-Widen et al., 2001; Norden & Godbout, 2013; Sasseville et al., 2012; Vite & Head, 2014; Wohlsein et al., 2012; Youssef et al., 2016). In the present study, reactive astrocytosis was always associated with increased levels of WM vacuolation. While this may be incidental, it could also reflect another underlying pathological process, such as age-related neurodegeneration. Within the CNS, neuroglial cells, especially astrocytes, react promptly (Peters et al., 1976). It seems possible that the astrogliosis seen occasionally in our study was in response to either neural tissue damage associated to *P. multocida* infection, as sequela to nonspecific sepsis leading to neuroinflammation and ischemia, or in response to subtle age-related background degeneration of myelin sheaths and/or neuronal cell processes.

Perivascular ceroid, a yellow pigment similar to lipofuscin that is found in macrophages, was observed in all monkey brains. Perivascular ceroid-laden macrophages have been described in the brain of aged humans (Neltner et al., 2015). Abnormal inclusions and debris have been described in perivascular neuroglial cells and pericytes of aged rhesus macaques, which were not specifically characterized but may represent hemosiderin or ceroid deposition (Hof et al., 2002). Perivascular macrophages containing ceroid accumulate in the WM of aged dogs, suggesting that the ceroid originates from degenerating myelin lipids (Chambers et al., 2012; Youssef et al., 2016). Our results are not consistent with this possible explanation, as ceroid-laden macrophages were observed in all monkeys, including those with minimal WM vacuolation.

Meningeal and perivascular melanosis was a non-age-related finding that has also been described in humans, NHPs, and other animal species (Chamanza et al., 2010; Fankhauser, 1968; Goldgeier et al., 1984; Gudjohnsen et al., 2015; Wohlsein et al., 2012). Melanocytic cells are a normal finding within the subarachnoid space of the CNS, and their presence, albeit interpreted as of no pathological significance, can pose a theoretical risk for the development of meningeal melanocytic neoplasms (Goldgeier et al., 1984).

Intramural vascular mineralization is generally considered an incidental finding, although the pathogenesis and clinical impact of these dystrophic vascular deposits remain widely undetermined. Often not associated with abnormal clinical or histopathological findings, neurological signs and focal ischemia have occasionally been reported in association with severe vascular mineralization and stenosis (Martínez et al., 2012; Youssef et al., 2016). Vascular mineralization has been described in humans, aged rhesus macaques, and many other animal species (Fankhauser, 1968; Gavier-Widen et al., 2001; Jahns, Callanan, McElroy, et al., 2006; Jeffrey, 1992; Lowe et al., 1997; Mandara et al., 2001; Wadsworth et al., 1995; Yanai et al., 1987, 1994; Youssef et al., 2016). While we did not find a statistically significant age relationship for vascular mineralization ($p = .1171$), we only observed this pathology in seven out of 71 animals, so we hypothesize that in a larger group, statistical results may be different.

Our study evaluated the largest group of AGMs for AD-related pathology to date. The age-related accumulation and progression of Aβ plaques suggest that in this species, scattered extracellular Aβ can be detected in neuropil between 10 and 15 years of age, and that discrete Aβ plaques are primarily detected after the age of 15 years. This age range of initial detection of extracellular Aβ is consistent with previous findings by Kalinin and colleagues (2013), in which low numbers of small Aβ(6E10)-ir plaques with diffusely stained morphology were detected in four out of five younger AGMs (10.8 ± 0.4 years) (Kalinin et al., 2013). Kumar et al. (2018) also report similar findings with small levels of Aβ detected in three out of six monkeys 11–15 years of age, and more prominent Aβ in eight out of nine monkeys 15–32 years of age (Kumar et al., 2018). Our observations support the concept that initial diffuse extracellular accumulations in young AGMs precede Aβ plaque formation in older animals, which increase in expression profile, size, and quantity with age. Additionally, three of the four middle-aged monkeys with scattered extracellular Aβ also demonstrated mild levels of CP13-ir for p-tau, further supporting the notion that these middle-aged monkeys displayed early AD-like pathology that progresses with age.

In our study, Aβ-ir plaques were observed, using 4G8 antibody, in the PFC, FC, CC, and TC, which is consistent with previous AGM findings (Cramer et al., 2018; Kalinin et al., 2013; Kumar et al., 2018; Latimer et al., 2018; Lemere et al., 2004). In humans, Aβ pathology in these isocortical lobes of the brain (neocortex) is generally considered the earliest stage of AD (Serrano-Pozo et al., 2011). In one aged female AGM (estimated to be 25 years old), Aβ plaques were also

detected in the EC. In AD progression, the EC, along with the hippocampus, is generally believed to develop plaques later than the neocortex (Serrano-Pozo et al., 2011). This particular monkey (No. 111) displayed the most abundant p-tau CP13-ir profiles in the MTL, suggesting this individual had the most advanced AD-like pathology in the study.

Aβ plaques were roughly round and had an average diameter of 70 μm, and many plaques were dense with a central core; others were more diffuse with a granular appearance, a morphology corresponding to early plaques in AD patients (Akiyama et al., 1999). Interestingly, the previously described focal areas of eosinophilic pallor observed in the neuropil of the cerebral cortex with H&E stain were exclusively seen in the 10 monkeys with Aβ-ir plaques. These pale foci within the neuropil, although not observed with the same frequency, corresponded topographically to 4G8-ir plaques. This previously unreported association suggests that, in some instances, Aβ plaques in the brain of aging AGMs may be detected using routine H&E staining as poorly defined pale-stained foci, potentially caused by changes in stain uptake at the regions where Aβ deposits become denser. These foci were smaller (approximately 20–80 μm in diameter) than many Aβ plaques identified by IHC, which may suggest they represent the dense core of the plaques. To our knowledge, although cortical Aβ plaques have been recognized on H&E-stained sections of human brains (Serrano-Pozo et al., 2011), this is a novel potentially diagnostic finding in NHPs.

Increased numbers of reactive astrocytes detected by GFAP immunostaining were observed in immune-stained tissue adjacent to Aβ plaques in all 10 monkeys, suggestive of plaque-associated inflammation, and consistent with previous findings in humans and AGMs (Cramer et al., 2018; Kalinin et al., 2013; Kamphuis et al., 2014; Lemere et al., 2004). In AD, classic plaques have a core of Aβ_{40} and A$\beta_{42/43}$ polymers, activated microglial cells, and reactive astrocytes found more abundantly at the periphery of the plaque. Other proteins and chemicals co-localize with these plaques, including neurotransmitters, cytoskeletal and transmembrane proteins, acute phase inflammatory proteins and immunoglobulins, growth factors, digestive enzymes, G-protein cascade participants, and a range of phospholipid-derived molecules (Armstrong, 2009; Zhu et al., 2004). Inflammation, characterized by sustained activation of immunocytes and cytokine dysregulation exacerbating Aβ and tau pathology, is thought to play a significant role in the pathogenesis of AD (Kinney et al., 2018).

Intramural vascular Aβ-ir profiles increased significantly with age and were detected in both parenchymal and surface blood vessels, most frequently in the PFC but also in the FC and TC and, rarely, within cortical WM tracts. In addition, Aβ-containing blood vessels were likely co-localized with GFAP expression, which would indicate an associated inflammatory response. These findings are consistent with previously reported vascular amyloid deposition in the AGM (Kumar et al., 2018; Lemere et al., 2004). In AD, vascular Aβ deposition, often termed "cerebral amyloid angiopathy," occurs throughout gray matter and leptomeninges. CAA is detected in 10–40% of aged human brains and in over 80% of the brains of AD patients. Local inflammation and vasculitis are also associated with vascular amyloid deposition. Amyloid deposits trigger a variety of molecular events within the brain, which may lead to the release of inflammatory mediators, oxidative stress, changes in permeability of the BBB, and ultimately to neuronal cell death. Mild CAA does not usually interfere with cerebrovascular function, as endothelial cells are not affected. However, as amyloid accumulation overwhelms vessel walls, spontaneous vascular rupture can occur, resulting in microhemorrhages and occasional larger "lobar" hemorrhages, which can be fatal. Small perivascular leakage and hemorrhages are frequently observed around vessels affected by CAA. Amyloid deposits can also lead to obstruction of the vessel lumen, resulting in regional ischemia and infarction. Neurological deficits, changes in consciousness, cognitive change, dementia, and death have all been associated with severe CAA (Biffi & Greenberg, 2011).

Our study is the first to use 4G8 antibody to detect amyloid plaques in the AGM. Previously published studies have primarily worked with 6E10 antibody, and to a lesser extent antibodies against Aβ_{40} and Aβ_{42}, as well as pSer8Aβ for phosphorylated Aβ and npAβ against non-phosphorylated Aβ (Cramer et al., 2018; Kalinin et al., 2013; Kumar et al., 2018; Latimer et al., 2018; Lemere et al., 2004). Our findings are mostly consistent with previous literature, which suggests 4G8 is a good alternative antibody for amyloid detection in the aged AGM brain. Many of these antibodies have some level of cross-reactivity with other proteins; specifically, 4G8 cross-reacts with P3 and with conformational epitope of aggregated fibrils including α-synuclein (Hunter & Brayne, 2017). These four antibodies targeting amino acid residues present in Aβ consistently stain extracellular Aβ deposits. Finally, 4G8 and 6E10 both cross-react with APP; therefore, these antibodies cannot accurately evaluate intracellular Aβ levels (Aho et al., 2010).

Tau phosphorylation was more prominent in middle-aged and older animals than in the youngest group. In the aged AGMs, CP13-ir profiles appeared to have stronger immunoreactivity and more extended distribution compared to the youngest and middle-aged monkeys in most of the anatomical regions examined. Tau phosphorylation is an early event in NFT formation, as hyperphosphorylation impairs the microtubule binding function of tau, resulting in the destabilization of microtubules within neurons. Eventually, tau detaches from the microtubules, aggregates and assembles into NFTs that impair axonal transport, and ultimately results in neuronal degeneration (Sanabria-Castro et al., 2017). CP13 antibody detects p-tau at Ser202 at an early nonfibrillary pretangle state, and at the later stage in which neurons contained NFTs (Andorfer et al., 2003). Here, we have observed soluble phosphorylated granular tau within neurons, oligodendrocytes, and processes, but not NFTs, indicative of an early tau pathology in AGMs. Our findings are consistent with previous findings in the AGM and other NHPs that have identified p-tau at a pretangle state, without evidence of true NFTs (Cramer et al., 2018; Edler et al., 2017; Gearing et al., 1994; Heuer et al., 2012; Latimer et al., 2018; Lemere et al., 2004; Oikawa et al., 2010; Perez et al., 2013, 2016; Schultz et al., 2000). As AGMs do have a potential life span of over 30 years, it is possible that our monkeys were not old enough to detect the NFT formation. Interestingly, in vitro studies have demonstrated that tau phosphorylation at Ser202 site is key for promoting tau fibrils (Despres et al., 2017; Xia et al., 2020), additionally supporting the use of the AGM as a naturally

occurring model of early tau pathology. Recently, we have demonstrated that the intrathecal injection of oligomeric Aβ (AβO) in young AGMs led to increases of tau phosphorylation in the MTL using the AT8 antibody, supporting the value of this translational model of AD (Wakeman et al., 2022). The discrepancy between Wakeman's work and our findings showing the absence of tau-phosphorylated AT8-positive profiles in AGMs is most likely due to differential aspects of tissue processing (e.g., immersion vs. perfusion-fixed, long postmortem intervals, paraffin embedded tissue vs. frozen cut) that is known to affect the antigenicity of specific phospho-tau epitopes (Garver et al., 1994; Oh et al., 2010; Riederer et al., 1993). It is possible that during fixation or long postmortem intervals, the proteolysis or dephosphorylation of the tau phosphoepitopes recognized by AT8 occurs prior to full fixation of the tissue. This could explain the presence of tau phosphoepitope at Ser202 site detected by CP13 (pSer202), but not at Thr205 site, as AT8 failed to expose the dual tau phosphoepitope at Ser202 and Thr205 sites in our AGMs, suggesting that AT8 phosphoepitope is more susceptible to be destroyed during tissue processing than CP13 in AGMs brains (Garver et al., 1994; Oh et al., 2010; Riederer et al., 1993). Further studies are needed to understand the impact of fixation on early tau phosphorylation in AGMs.

We also detected CP13 immunostaining in oligodendrocyte-like cells near neurons within gray matter in the FC and MTL as well as within WM. This finding has previously been reported in cynomolgus macaques, baboons, and gorillas (Oikawa et al., 2010; Perez et al., 2013, 2016; Schultz et al., 2000). In humans with tauopathies and AD, tau aggregation within astrocytes and oligodendrocytes is not uncommon; however, the significance and role of both neuroinflammation and glial tau accumulations in the pathogenesis of AD are currently under review. WM damage has also been shown to emerge prior to amyloid and plaque pathology in AD patients (Xiao, 2016), and microglial density and astrocytic activation within WM are increased compared to age-matched controls (Liu et al., 2016). The aged AGM, therefore, may serve as a model to further investigate these changes, due to the abundance of age-related WM and glial changes observed by histopathology in our AGM brains along with the detection of tau phosphorylation within glial cells. To our knowledge, p-tau in glial cells in the AGM has not previously been reported.

Five of our aged animals demonstrated a wide spectrum of AD-like pathology, including Aβ plaques with likely co-localized inflammation, CAA, and p-tau. Overall, these findings suggest that these aged animals can serve as an important model for the evaluation of potential AD therapeutics. Recently, an induced AGM model of AD has been developed using intrathecal injection of AβOs (Wakeman et al., 2022). Our description of naturally occurring background neuropathology in the untreated AGM brain ($n = 71$) will enhance interpretation of observed neuropathology findings in this novel AβO-induced animal model, and application of the model, including guiding age criteria for study recruitment and powering sufficiently to account for the natural incidence of pathology. Additionally, candidate therapeutics showing promise in the induced model have the potential to undergo follow-up testing in the scarce and valuable naturally occurring AGM model of AD and CAA.

All monkeys included in the study were under veterinary supervision and did not exhibit overt clinical signs of neurologic disease prior to death. All but four brains were collected from euthanized animals enrolled across a wide spectrum of experiments that were deemed unlikely to impact the brain; many of the selected animals had been enlisted in ophthalmology studies. It is possible that the reported optic tract vacuolation could have been influenced by these studies; however, more than 10 different ophthalmic experiments with varying interventions and test articles were represented in these monkeys, and it is highly unlikely that they would all result in the same microscopic change to the optic tract. Furthermore, this finding was also observed in monkeys with no history of ophthalmic intervention and has previously been reported in the clinically normal rhesus monkey (Hof et al., 2002). Most of the aged monkeys in this study were members of the SKBRF AGM breeding colony and had minimal prior study history, outside of noninvasive studies characterizing the aged AGM. Specimens were collected opportunistically over 3 years; therefore, brains were subjected to slightly different tissue processing protocols. However, our histological findings were consistent across different studies, which suggests that such changes are present in the AGM brain regardless of clinical history, study enrollment, or slight variations in histological tissue processing protocols.

Most monkeys on this study were wild caught, and as a result their ages were estimates. Although age estimates were performed using an internal protocol thought to be reasonably accurate, this limitation may have introduced some variability to the data. The large group size, however, helped to mitigate the impact of variability among individual monkeys. One aged monkey was colony born and had a known age of 25 years; seven other aged monkeys had been in the colony for years and had a minimum verifiable age. Of note, this study represents one of the only evaluations of wild-caught AGMs for AD-like pathology, and our results, both in observed pathology and age of onset, are comparable to those obtained from purpose-bred populations. An additional study limitation was that, because of random specimen availability, the ratio of males to females within each group was not well-balanced, with an overall ratio of M:F of 47:24. AD pathology is known to be more common in females, with two out of three late-onset cases affecting women (Alzheimer's Association, 2020). Although it has not been previously reported, it is possible that this gender association exists in the AGM as well, in which case a higher representation of males in younger groups and higher representation of females in the oldest group could have somehow influenced our results.

5 | CONCLUSION

The evaluation of a large group of AGM brains in this study highlighted numerous background histopathologic findings that can now be classified as age related or non-age related, similar to those found in humans and other animal species. Recognizing these findings and their anatomical distribution and frequency will benefit neuropathologists, and those working with AGMs in the biomedical and pharmaceutical research setting, with the microscopic assessment of the brain in this

species. The evaluation of the largest reported group to date of wild-caught AGMs for the presence of AD-related pathology confirmed previous findings in purpose-bred populations of age-related cerebrocortical Aβ plaque formation and vascular Aβ deposition associated with concomitant focally increased GFAP immunostaining. We demonstrated that distinct Aβ plaques are not seen in AGMs under the age of 10 years and are rarely detected in animals under the age of 15 years, although scattered extracellular Aβ immunoreactivity can be found in animals over the age of 10 years. We also demonstrate tau phosphorylation primarily in middle-aged and aged AGMs in neurons, neuropil, and glial cells of the neocortex and limbic system. These findings document important differences between the aged AGM brain and the brain of human patients diagnosed with AD, but also identify similarities that support the relevance of the AGM as a model for AD research and advance our knowledge of background neuropathology associated with normal aging in this NHP species.

ACKNOWLEDGMENTS

The authors would like to thank David Hilchie for performing the histology processing and special stains; Histo-Scientific Research Laboratories for performing immunohistochemistry; Behavioural Science Foundation (St. Kitts) and Amy Beierschmitt for contributing brain samples; veterinary team and staff at St. Kitts Biomedical Research Foundation for their technical support; Maurice Matthew for his assistance with tissues processing; and Dustin Wakeman and John Elsworth for their contribution to the manuscript development.

CONFLICT OF INTEREST STATEMENT

Three authors are Virscio employees and have the commercial interest in providing primate translational research.

DATA AVAILABILITY STATEMENT

Additional data will be provided upon request.

ORCID

Tatiana M. Corey https://orcid.org/0000-0002-3131-1034

PEER REVIEW

The peer review history for this article is available at https://publons.com/publon/10.1002/cne.25494.

REFERENCES

Aho, L., Pikkarainen, M., Hiltunen, M., Leinonen, V., & Alafuzoff, I. (2010). Immunohistochemical visualization of amyloid-β protein precursor and amyloid-β in extra- and intracellular compartments in the human brain. *Journal of Alzheimer's Disease*, *20*, 1015–1028. https://doi.org/10.3233/JAD-2010-09168110.3233/JAD-2010-091681

Akiyama, H., Mori, H., Saido, T., Kondo, H., Ikeda, K., & McGeer, P. L. (1999). Occurrence of the diffuse amyloid beta-protein (Abeta) deposits with numerous Abeta-containing glial cells in the cerebral cortex of patients with Alzheimer's disease. *Glia*, *25*(4), 324–331. https://doi.org/10.1002/(SICI)1098-1136(19990215)25:4%3c324::AID-GLIA2%3e3.0.CO;2-5

Alzheimer's Association. (2020). 2020 Alzheimer's disease facts and figures. *Alzheimer's & Dementia*, *16*(3), 391–460.

Andorfer, C., Kress, Y., Espinoza, M., De Silva, R., Tucker, K. L., Barde, Y.-A., Duff, K., & Davies, P. (2003). Hyperphosphorylation and aggregation of tau in mice expressing normal human tau isoforms. *Journal of Neurochemistry*, *86*, 582–590. https://doi.org/10.1046/j.1471-4159.2003.01879.x10.1046/j.1471-4159.2003.01879.x

Armstrong, R. (2009). The molecular biology of senile plaques and neurofibrillary tangles in Alzheimer's disease. *Folia Neuropathologica*, *47*(4), 289–299.

Beech, J. (1984). Neuroaxonal dystrophy of the accessory cuneate nucleus in horses. *Veterinary Pathology*, *21*, 384–393. https://doi.org/10.1177/030098588402100404 10.1177/030098588402100404

Benedikz, E., Kloskowska, E., & Winblad, B. (2009). The rat as an animal model of Alzheimer's disease. *Journal of Cellular and Molecular Medicine*, *13*(6), 1034–1042. https://doi.org/10.1111/j.1582-4934.2009.00781.x10.1111/j.1582-4934.2009.00781.x

Biffi, A., & Greenberg, S. M. (2011). Cerebral amyloid angiopathy: A systematic review. *Journal of Clinical Neurology*, *7*(1), 1–9. https://doi.org/10.3988/jcn.2011.7.1.110.3988/jcn.2011.7.1.1

Borràs, D., Ferrer, I., & Pumarola, M. (1999). Age-related changes in the brain of the dog. *Veterinary Pathology*, *36*, 202–211. https://doi.org/10.1354/vp.36-3-20210.1354/vp.36-3-202

Brannon, W., Mccormick, W., & Lampert, P. (1967). Axonal dystrophy in the gracile nucleus of man. *Acta Neuropathologica*, *9*, 1–6. https://doi.org/10.1007/BF0068815310.1007/BF00688153

Bronson, R. T., & Schoene, W. C. (1980). Spontaneous pallido-nigral accumulation of iron pigment and spheroid-like structures in macaque monkeys. *Journal of Neuropathology and Experimental Neurology*, *39*(2), 181–196. https://doi.org/10.1097/00005072-198003000-0000710.1097/00005072-198003000-00007

Capucchio, M. T., Márquez, M., Pregel, P., Foradada, L., Bravo, M., Mattutino, G., Torre, C., Schiffer, D., Catalano, D., Valenza, F., Guarda, F., & Pumarola, M. (2010). Parenchymal and vascular lesions in ageing equine brains: Histological and immunohistochemical studies. *Journal of Comparative Pathology*, *142*(1), 61–73. https://doi.org/10.1016/j.jcpa.2009.07.00710.1016/j.jcpa.2009.07.007

Chamanza, R., Marxfeld, H. A., Blanco, A. I., Naylor, S. W., & Bradley, A. E. (2010). Incidences and range of spontaneous lesions in control cynomolgus monkeys (*Macaca fascicularis*) used in toxicity studies. *Toxicologic Pathology*, *38*, 642–657. https://doi.org/10.1177/019262331036898110.1177/0192623310368981

Chambers, J., Tokuda, T., Uchida, K., Ishii, R., Tatebe, H., Takahashi, E., Tomiyama, T., Une, Y., & Nakayama, H. (2015). The domestic cat as a natural animal model of Alzheimer's disease. *Acta Neuropathologica Communications*, *3*(78), 1–14.

Chambers, J. K., Uchida, K., & Nakayama, H. (2012). White matter myelin loss in the brains of aged dogs. *Experimental Gerontology*, *47*, 263–269. https://doi.org/10.1016/j.exger.2011.12.00310.1016/j.exger.2011.12.003

Collier, T. J., Redmond, D. E., Steece-Collier, K., Lipton, J. W., & Manfredsson, F. P. (2016). Is alpha-synuclein loss-of-function a contributor to parkinsonian pathology? Evidence from non-human primates. *Frontiers in Neuroscience*, *10*, 1–12. https://doi.org/10.3389/fnins.2016.0001210.3389/fnins.2016.00012

Cork, L., & Walker, L. (1993). Age-related lesions, nervous system. In T. C. Jones, U. Mohr, & R. D. Hunt (Eds.), *Nonhuman primates. Monographs on pathology of laboratory animals* (Vol. 2, pp. 173–183). Springer. https://doi.org/10.1007/978-3-642-84924-4_3710.1007/978-3-642-84924-4_37

Cramer, P. E., Gentzel, R. C., Tanis, K. Q., Vardigan, J., Wang, Y., Connolly, B., Manfre, P., Lodge, K., Renger, J. J., Zerbinatti, C., & Uslaner, J. M. (2018). Aging African green monkeys manifest transcriptional, pathological, and cognitive hallmarks of human Alzheimer's disease. *Neurobiology of Aging*, *64*, 92–106. https://doi.org/10.1016/j.neurobiolaging.2017.12.01110.1016/j.neurobiolaging.2017.12.011

De La Monte, S. M., & Wands, J. R. (2008). Alzheimer's disease is type 3 diabetes-evidence reviewed. *Journal of Diabetes Science and Technology*, *2*(6), 1101–1113. https://doi.org/10.1177/193229680800200619 10.1177/193229680800200619

Despres, C., Byrne, C., Qi, H., Cantrelle, F.-X., Huvent, I., Chambraud, B., Baulieu, E.-E., Jacquot, Y., Landrieu, I., Lippens, G., & Smet-Nocca, C. (2017). Identification of the Tau phosphorylation pattern that drives its aggregation. *Proceedings of the National Academy of Sciences of the United States of America*, *114*(34), 9080–9085. https://doi.org/10.1073/pnas.1708448114 10.1073/pnas.1708448114

Edler, M. K., Sherwood, C. C., Meindl, R. S., Hopkins, W. D., Ely, J. J., Erwin, J. M., Mufson, E. J., Hof, P. R., & Raghanti, M. A. (2017). Aged chimpanzees exhibit pathologic hallmarks of Alzheimer's disease. *Neurobiology of Aging*, *59*(Nov), 107–120. https://doi.org/10.1016/j.neurobiolaging.2017.07.006 10.1016/j.neurobiolaging.2017.07.006

Elsworth, J. D., Taylor, J. R., Sladek, J. R., Collier, T. J., Redmond, D. E., & Roth, R. H. (2000). Striatal dopaminergic correlates of stable parkinsonism and degree of recovery in old-world primates one year after MPTP treatment. *Neuroscience*, *95*(2), 399–408. https://doi.org/10.1016/S0306-4522(99)00437-6 10.1016/S0306-4522(99)00437-6

Fainman, J., Eid, M.-D., Ervin, F. R., & Palmour, R. M. (2007). A primate model for Alzheimer's disease: Investigation of the apolipoprotein E profile of the vervet monkey of St. Kitts. *American Journal of Medical Genetics, Part B, Neuropsychiatric Genetics*, *144B*, 818–819. https://doi.org/10.1002/ajmg.b.30276 10.1002/ajmg.b.30276

Fankhauser, R. L. H. (1968). Zentrales nervensystem. In J. Dobberstein & H. Stünzi (Eds.), *Handbuch der speziellen pathologischen Anatomie der Haustiere* (Vol. 3, pp. 191–436). Cornell University is the publication, Parey.

Forny-Germano, L., Lyra E Silva, N. M., Batista, A. F., Brito-Moreira, J., Gralle, M., Boehnke, S. E., Coe, B. C., Lablans, A., Marques, S. A., Martinez, A. M. B., Klein, W. L., Houzel, J.-C., Ferreira, S. T., Munoz, D. P., & De Felice, F. G. (2014). Alzheimer's disease-like pathology induced by amyloid-β oligomers in nonhuman primates. *Journal of Neuroscience*, *34*(41), 13629–13643. https://doi.org/10.1523/JNEUROSCI.1353-14.2014 10.1523/JNEUROSCI.1353-14.2014

Fujisawa, K. (1967). AN UNIQUE TYPE OF AXONAL ALTERATION (so-called axonal dystrophy) as seen in Goll's nucleus of 277 cases of controls. A contribution to the pathology of aging process. *Acta Neuropathologica*, *8*(3), 255–275. https://doi.org/10.1007/BF00688827 10.1007/BF00688827

Garver, T. D., Harris, K. A., Lehman, R. A. W., Lee, V. M.-Y., Trojanowski, J. Q., & Billingsley, M. L. (1994). Tau phosphorylation in human, primate, and rat brain: Evidence that a pool of tau is highly phosphorylated in vivo and is rapidly dephosphorylated in vitro. *Journal of Neurochemistry*, *63*(6), 2279–2287. https://doi.org/10.1046/j.1471-4159.1994.63062279.x10.1046/j.1471-4159.1994.63062279.x

Gavier-Widen, D., Wells, G. A. H., Simmons, M. M., Wilesmith, J. W. W., & Ryan, J. (2001). Histological observations on the brains of symptomless 7-year-old cattle. *Journal of Comparative Pathology*, *124*, 52–59. https://doi.org/10.1053/jcpa.2000.0428 10.1053/jcpa.2000.0428

Gearing, M., Rebeck, G. W., Hyman, B. T., Tigges, J., & Mirra, S. S. (1994). Neuropathology and apoliporotein E profile of aged chimpanzees: Implications for Alzheimers disease. *Proceedings National Academy of Science of the United States of America*, *91*, 9382–9386. https://doi.org/10.1073/pnas.91.20.938210.1073/pnas.91.20.9382

Goldgeier, M. H., Klein, L. E., Klein-Angerer, S., Moellmann, G., & Nordlund, J. J. (1984). The distribution of melanocytes in the leptomeninges of the human brain. *Journal of Investigative Dermatology*, *82*(3), 235–238. https://doi.org/10.1111/1523-1747.ep1226011110.1111/1523-1747.ep12260111

Grinberg, L. T., & Thal, D. R. (2010). Vascular pathology in the aged human brain. *Acta Neuropathologica*, *119*(3), 277–290. https://doi.org/10.1007/s00401-010-0652-710.1007/s00401-010-0652-7

Gudjohnsen, S. A. H., Atacho, D. A. M., Gesbert, F., Raposo, G., Hurbain, I., Larue, L., Steingrimsson, E., & Petersen, P. H. (2015). Meningeal melanocytes in the mouse: Distribution and dependence on Mitf. *Frontiers in Neuroanatomy*, *9*, 149. https://doi.org/10.3389/fnana.2015.0014910.3389/fnana.2015.00149

Haines, D. E. (2000). Neuroanatomy: An atlas of structures, sections, and systems. Lippincott Williams & Wilkins.

Herrero, M. T., Hirsch, E. C., Kastner, A., Luquin, M. R., Javoy-Agid, F., Gonzalo, L. M., Obeso, J. A., & Agid, Y. (1993). Neuromelanin accumulation with age in catecholaminergic neurons from *Macaca fascicularis* brainstem. *Developmental Neuroscience*, *15*, 37–48. https://doi.org/10.1159/00011131510.1159/000111315

Heuer, E., Jacobs, J., Du, R., Wang, S., Keifer, O. P., Cintron, A. F., Dooyema, J., Meng, Y., Zhang, X., & Walker, L. C. (2017). Amyloid-related imaging abnormalities in an aged squirrel monkey with cerebral amyloid angiopathy. *Journal of Alzheimer's Disease*, *57*(2), 519–530. https://doi.org/10.3233/JAD-16098110.3233/JAD-160981

Heuer, E., Rosen, R. F., Cintron, A., & Walker, L. C. (2012). Nonhuman primate models of Alzheimer-like cerebral proteopathy. *Current Pharmaceutical Design*, *18*(8), 1159–1169. https://doi.org/10.2174/138161212799315885 10.2174/138161212799315885

Hiroaki, F., Fukumoto, H., Rosene, D. L., Moss, M. B., Raju, S., Hyman, B. T., & Irizarry, M. C. (2004). ß-Secretase activity increases with aging in human, monkey, and mouse brain. *American Journal of Pathology*, *164*(2), 719–725.

Hof, P., Gilissen, E. P., Sherwood, C. C., Duan, H., Lee, P. W. H., Delman, B. N., Naidich, T. P., Gannon, P. J., Perl, D. P., & Erwin, J. M. (2002). Comparative neuropathology of brain aging in primates. In J. M. Erwin & P. R. Hof (Eds.), *Aging in nonhuman primates* (pp. 130–154). Karger.

Hooper, P. T. (1999). Incidental lesions in the brain of sheep and goats. *Australian Veterinary Journal*, *77*, 398–399. https://doi.org/10.1111/j.1751-0813.1999.tb10316.x10.1111/j.1751-0813.1999.tb10316.x

Horvath, T. L., Diano, S., Leranth, C., Garcia-Segura, L. M., Cowley, M. A., Shanabrough, M., Elsworth, J. D., Sotonyi, P., Roth, R. H., Dietrich, E. H., Matthews, R. T., Barnstable, C. J., & Redmond, D. E (2003). Coenzyme Q induces nigral mitochondrial uncoupling and prevents dopamine cell loss in a primate model of Parkinson's disease. *Endocrinology*, *144*(7), 2757–2760. https://doi.org/10.1210/en.2003-016310.1210/en.2003-0163

Hunter, S., & Brayne, C. (2017). Do anti-amyloid beta protein antibody cross reactivities confound Alzheimer disease research? *Journal of Negative Results in Biomedicine*, *16*(1), 1. https://doi.org/10.1186/s12952-017-0066-310.1186/s12952-017-0066-3

Hurley, P. J., Elsworth, J. D., Whittaker, M. C., Roth, R. H., & Redmond, D. E. (2011). Aged monkeys as a partial model for Parkinson's disease. *Pharmacology Biochemistry and Behavior*, *99*(3), 324–332. https://doi.org/10.1016/j.pbb.2011.05.00710.1016/j.pbb.2011.05.007

International Union for Conservation of Nature (IUCN). (2022). *IUCN Red List of Threatened Species. Version 2017-2*. www.iucnredlist.org

Jahns, H., Callanan, J. J., McElroy, M. C., Sammin, D. J., & Bassett, H. F. (2006). Age-related and non-age-related changes in 100 surveyed horse brains. *Veterinary Pathology*, *43*, 740–750. https://doi.org/10.1354/vp.43-5-74010.1354/vp.43-5-740

Jahns, H., Callanan, J. J., Sammin, D. J., Mcelroy, M. C., & Bassett, H. F. (2006). Survey for transmissible spongiform encephalopathies in Irish pigs fed meat and bone meal. *The Veterinary Record*, *159*(5), 137–142. https://doi.org/10.1136/vr.159.5.13710.1136/vr.159.5.137

Jasinska, A. J., Lin, M. K., Service, S., Choi, O.-W., Deyoung, J., Grujic, O., Kong, S.-Y., Jung, Y., Jorgensen, M. J., Fairbanks, L. A., Turner, T., Cantor, R. M., Wasserscheid, J., Dewar, K., Warren, W., Wilson, R. K., Weinstock, G., Jentsch, J. D., & Freimer, N. B. (2012). A non-human primate system for large-scale genetic studies of complex traits. *Human Molecular*

Genetics, *21*(15), 3307–3316. https://doi.org/10.1093/hmg/dds16010.1093/hmg/dds160

Jeffrey, M. (1992). A neuropathological survey of brains submitted under the bovine spongiform encephalopathy orders in Scotland. *The Veterinary Record*, *131*, 332–337. https://doi.org/10.1136/vr.131.15.33210.1136/vr.131.15.332

Jellinger, K., & Jirásek, A. (1971). Neuroaxonal dystrophy in man: Character and natural history. *Acta Neuropathologica*, *5*(Suppl. 5), 3–16.

Kalinin, S., Willard, S. L., Shively, C. A., Kaplan, J. R., Register, T. C., Jorgensen, M. J., Polak, P. E., Rubinstein, I., & Feinstein, D. L. (2013). Development of amyloid burden in African green monkeys. *Neurobiology of Aging*, *34*(10), 2361–2369. https://doi.org/10.1016/j.neurobiolaging.2013.03.02310.1016/j.neurobiolaging.2013.03.023

Kamphuis, W., Middeldorp, J., Kooijman, L., Sluijs, J. A., Kooi, E.-J., Moeton, M., Freriks, M., Mizee, M. R., & Hol, E. M. (2014). Glial fibrillary acidic protein isoform expression in plaque related astrogliosis in Alzheimer's disease. *Neurobiology of Aging*, *35*(3), 492–510. https://doi.org/10.1016/j.neurobiolaging.2013.09.03510.1016/j.neurobiolaging.2013.09.035

Kikuchi, K. (1928). Über die altersveränderungen am gehirn des pferdes. *Arch Tierheilkunde*, *58*, 541–573.

Kimura, N., Nakamura, S., Goto, N., Narushima, E., Hara, I., Shichiri, S., Saitou, K., Nose, M., Hayashi, T., Kawamura, S., & Yoshikawa, Y. (2001). Senile plaques in an aged western lowland gorilla. *Experimental Animals*, *50*(1), 77–81. https://doi.org/10.1538/expanim.50.7710.1538/expanim.50.77

Kinney, J. W., Bemiller, S. M., Murtishaw, A. S., Leisgang, A. M., Salazar, A. M., & Lamb, B. T. (2018). Inflammation as a central mechanism in Alzheimer's disease. *Alzheimer's & Dementia*, *4*, 575–590. https://doi.org/10.1016/j.trci.2018.06.01410.1016/j.trci.2018.06.014

Kumar, S., Frost, J. L., Cotman, C. W., Head, E., Palmour, R., Lemere, C. A., & Walter, J. (2018). Deposition of phosphorylated amyloid-β in brains of aged nonhuman primates and canines. *Brain Pathology*, *28*(3), 427–430. https://doi.org/10.1111/bpa.1257310.1111/bpa.12573

Lam, D., Jim, J., To, E., Rasmussen, C., Kaufman, P. L., & Matsubara, J. (2009). Astrocyte and microglial activation in the lateral geniculate nucleus and visual cortex of glaucomatous and optic nerve transected primates. *Molecular Vision*, *15*, 2217–29.

Latimer, C., Shively, C. A., Keene, C. D., Jorgensen, M. J., Andrews, R. N., Register, T. C., Montine, T. J., Wilson, A. M., Neth, B. J., Mintz, A., Maldjian, J. A., Whitlow, C. T., Kaplan, J. R., & Craft, S. (2018). A nonhuman primate model of early Alzheimer's disease pathologic change: Implications for disease pathogenesis. *Alzheimer's & Dementia*, *15*(1), 93–105.

Lawrence, M. S., Redmond, D. E., Elsworth, J. D., Taylor, J. R., & Roth, R. H. (1991). The D1 receptor antagonist, SCH 23390, induces signs of parkinsonism in African green monkeys. *Life Sciences*, *49*, PL229–PL234. https://doi.org/10.1016/0024-3205(91)90299-Q10.1016/0024-3205(91)90299-Q

Lemere, C. A., Beierschmitt, A., Iglesias, M., Spooner, E. T., Bloom, J. K., Leverone, J. F., Zheng, J. B., Seabrook, T. J., Louard, D., Li, D., Selkoe, D. J., Palmour, R. M., & Ervin, F. R. (2004). Alzheimer's disease abeta vaccine reduces central nervous system abeta levels in a non-human primate, the Caribbean vervet. *American Journal of Pathology*, *165*(1), 283–297. https://doi.org/10.1016/S0002-9440(10)63296-810.1016/S0002-9440(10)63296-8

Liu, H., Yang, Y., Xia, Y., Zhu, W., Leak, R. K., Wei, Z., Wang, J., & Hu, X. (2016). Aging of cerebral white matter. *Ageing Research Reviews*, *34*, 64–76. https://doi.org/10.1016/j.arr.2016.11.00610.1016/j.arr.2016.11.006

Lowe, J., Lennox, G., & Leigh, N. (1997). Disorders of movement and system degenerations. In D. I. Graham & P. L. Lantos (Eds.), *Greenfield's neuropathology* (pp. 281–366). Arnold.

Mandara, M., Ricci, G., & Capuccini, S. (2001). *Blood vessel calcification in the brain of the cat: An age-related lesion*. Proceedings of the 19th Meeting ESVP 25-28 September; Thessaloniki, Greece: 198.

Marsden, C. (1961). Pigmentation in the nucleus substantiae nigrae of mammals. *Journal of Anatomy*, *95*(2), 256–261.

Martínez, J., Montgomery, D. L., & Uzal, F. A. (2012). Vascular mineralization in the brain of horses. *Journal of Veterinary Diagnostic Investigation*, *24*(3), 612–617. https://doi.org/10.1177/104063871244235210.1177/1040638712442352

Moreno-García, A., Kun, A., Calero, O., Medina, M., & Calero, M. (2018). An overview of the role of lipofuscin in age-related neurodegeneration. *Frontiers in Neuroscience*, *12*(464), 1–13.

Nanda, B. S., & Getty, R. (1971). Lipofuscin pigment in the nervous system of aging pig. *Experimental Gerontology*, *6*(6), 447–452. https://doi.org/10.1016/0531-5565(71)90023-410.1016/0531-5565(71)90023-4

National Research Council. (1981). *Techniques for the study of primate population ecology*. The National Academies Press.

Ndung'u, M., Härtig, W., Wegner, F., Mwenda, J. M., Low, R. W. C., Akinyemi, R. O., & Kalaria, R. N. (2012). Cerebral amyloid β(42) deposits and microvascular pathology in ageing baboons. *Neuropathology and Applied Neurobiology*, *38*(5), 487–499. https://doi.org/10.1111/j.1365-2990.2011.01246.x10.1111/j.1365-2990.2011.01246.x

Neltner, J. H., Abner, E. L., Jicha, G. A., Schmitt, F. A., Patel, E., Poon, L. W., Marla, G., Green, R. C., Davey, A., Johnson, M. A., Jazwinski, S. M., Kim, S., Davis, D., Woodard, J. L., Kryscio, R. J., Van Eldik, L. J., & Nelson, P. T. (2015). Brain pathologies in extreme old age. *Neurobiology of Aging*, *37*, 1–11. https://doi.org/10.1016/j.neurobiolaging.2015.10.00910.1016/j.neurobiolaging.2015.10.009

Newberne, J., Robinson, V., Estill, L., & Brinkman, D. (1960). Granular structures in the brain of apparently normal dogs. *American Journal of Veterinary Research*, *21*, 782–786.

Norden, D. M., & Godbout, J. P. (2013). Review: Microglia of the aged brain: Primed to be activated and resistant to regulation. *Neuropathology and Applied Neurobiology*, *39*(1), 19–34. https://doi.org/10.1111/j.1365-2990.2012.01306.x10.1111/j.1365-2990.2012.01306.x

Oh, K., Perez, S. E., Lagalwar, S., Vana, L., Binder, L., & Mufson, E. J. (2010). Staging of Alzheimer's pathology in triple transgenic mice: A light and electron microscopic analysis. *International Journal of Alzheimer's Disease*, *2010*, 780102.

Oikawa, N., Kimura, N., & Yanagisawa, K. (2010). Alzheimer-type tau pathology in advanced aged nonhuman primate brains harboring substantial amyloid deposition. *Brain Research*, *1315*, 137–149. https://doi.org/10.1016/j.brainres.2009.12.00510.1016/j.brainres.2009.12.005

Perez, S. E., Raghanti, M. A., Hof, P. R., Kramer, L., Ikonomovic, M. D., Lacor, P. N., Erwin, J. M., Sherwood, C. C., & Mufson, E. J. (2013). Alzheimer's disease pathology in the neocortex and hippocampus of the western lowland gorilla (*Gorilla gorilla gorilla*). *Journal of Comparative Neurology*, *521*(18), 4318–4338. https://doi.org/10.1002/cne.2342810.1002/cne.23428

Perez, S. E., Sherwood, C. C., Cranfield, M. R., Erwin, J. M., Mudakikwa, A., Hof, P. R., & Mufson, E. J. (2016). Early Alzheimer's disease-type pathology in the frontal cortex of wild mountain gorillas (*Gorilla beringei beringei*). *Neurobiology of Aging*, *39*, 195–201. https://doi.org/10.1016/j.neurobiolaging.2015.12.01710.1016/j.neurobiolaging.2015.12.017

Peters, A., Palay, S., & Webster, H. (1976). *The fine structure of the nervous system—The neurons and supporting cells*. W. B. Saunders Company.

Poduri, A., Gearing, M., Rebeck, G. W., Mirra, S. S., Tigges, J., & Hyman, B. T. (1994). Apolipoprotein E4 and beta amyloid in senile plaques and cerebral blood vessels of aged rhesus monkeys. *American Journal of Pathology*, *144*(6), 1183–1187.

Riederer, B. M., Porchet, R., Marugg, R. A., & Binder, L. I. (1993). Solubility of cytoskeletal proteins in immunohistochemistry and the influence of fixation. *Journal of Histochemistry and Cytochemistry*, *41*(4), 609–616. https://doi.org/10.1177/41.4.845020010.1177/41.4.8450200

Sanabria-Castro, A., Alvarado-Echeverría, I., & Monge-Bonilla, C. (2017). Molecular pathogenesis of Alzheimer's disease: An update. *Annals of Neurosciences*, *24*(1), 46–54. https://doi.org/10.1159/00046442210.1159/000464422

Santos, C., Snyder, P. J., Wu, W. C., Zhang, M., Echeverria, A., & Alber, J. (2017). Pathophysiologic relationship between Alzheimer's disease, cerebrovascular disease, and cardiovascular risk: A review and synthesis. *Alzheimer's & Dementia*, *7*, 69–87.

Sasseville, V. G., Mansfield, K. G., Mankowski, J. L., Tremblay, C., Terio, K. A., Mätz-Rensing, K., Gruber-Dujardin, E., Delaney, M. A., Schmidt, L. D., Liu, D., Markovits, J. E., Owston, M., Harbison, C., Shanmukhappa, S., Miller, A. D., Kaliyaperumal, S., Assaf, B. T., Kattenhorn, L., Macri, S. C., … Lowenstine, L. J. (2012). Meeting report: Spontaneous lesions and diseases in wild, captive-bred, and zoo-housed nonhuman primates and in nonhuman primate species used in drug safety studies. *Veterinary Pathology*, *49*(6), 1057–1069. https://doi.org/10.1177/0300985812461655 10.1177/0300985812461655

Schultz, C. (2000). Age-related progression of tau pathology in brains of baboons. *Neurobiology of Aging*, *21*(6), 905–912. https://doi.org/10.1016/S0197-4580(00)00176-7 10.1016/S0197-4580(00)00176-7

Serrano-Pozo, A., Frosch, M. P., Masliah, E., & Hyman, B. T. (2011). Neuropathological alterations in Alzheimer disease. *Cold Spring Harbor Perspectives in Medicine*, *1*(1), a006189. https://doi.org/10.1101/cshperspect.a006189 10.1101/cshperspect.a006189

Sharpe, J. (2004). Histopathological observations in the medulla oblongata of adult sheep at slaughter and sheep which died on farm. In *Studies on the diagnosis of transmissible spongiform* encephalopathies *in sheep* (PhD thesis) (pp. 34–42). Dublin, Ireland, University College Dublin.

Stepień, K., Dzierzega-Lecznar, A., & Tam, I. (2007). The role of neuromelanin in Parkinson's disease–new concepts (translation). *Wiadomosci Lekarskie*, *11*(12), 563–569.

Suzuki, Y., Ohta, K., & Suu, S. (1979). Correlative studies of axonal spheroids and lafora-like bodies in aged dogs. *Acta Neuropathologica*, *48*, 77–81. https://doi.org/10.1007/BF00691796 10.1007/BF00691796

Taylor, J. R., Lawrence, M. S., Redmond, D. E., Elsworth, J. D., Roth, R. H., Nichols, D. E., & Mailman, R. B. (1991). Dihydrexidine, a full dopamine D1 agonist, reduces MPTP-induced parkinsonism in monkeys. *European Journal of Pharmacology*, *199*(3), 389–391. https://doi.org/10.1016/0014-2999(91)90508-N 10.1016/0014-2999(91)90508-N

Vite, C. H., & Head, E. (2014). Aging in the canine and feline brain. *The Veterinary Clinics of North America: Small Animal Practice*, *44*, 1113–1129. https://doi.org/10.1016/j.cvsm.2014.07.008 10.1016/j.cvsm.2014.07.008

Wadsworth, P. F., Jones, H. B., & Cavanagh, J. B. (1995). The topography, structure and incidence of mineralized bodies in the basal ganglia of the brain of cynomolgus monkeys (*Macaca fascicularis*). *Laboratory Animals*, *29*, 276–281. https://doi.org/10.1258/002367795781088360 10.1258/002367795781088360

Wakeman, D., Weed, M. R., Perez, S. E., Cline, E. N., Viola, K. L., Wilcox, K. C., Moddrelle, D. S., Nisbett, E. Z., Kurian, A. M., Bell, A. F., Pike, R., Jacobson, P. B., Klein, W. L., Mufson, E. J., Lawrence, M. S., & Elsworth, J. D. (2022). Intrathecal amyloid-beta oligomer administration increases tau phosphorylation in the medial temporal lobe in the African green monkey: A nonhuman primate model of Alzheimer's disease. *Neuropathology and Applied Neurobiology*, *48*(e12800), 1–14.

Wohlsein, P., Deschl, U., & Baumgärtner, W. (2012). Nonlesions, unusual cell types, and postmortem artifacts of the central nervous system of domestic animals. *Veterinary Pathology*, *50*(1), 122–143. https://doi.org/10.1177/0300985812450719 10.1177/0300985812450719

Wolf, R., & White, G. (2012). Clinical techniques used for nonhuman primates. In C. Abee, K. Mansfield, S. Tardif, & T. Morris (Eds.), Nonhuman primates in biomedical research. Volume *1: Biology and management* (2nd ed., pp. 323–337). San Diego, CA, Elsevier.

Xia, Y., Prokop, S., Gorion, K.-M. M., Kim, J. D., Sorrentino, Z. A., Bell, B. M., Manaois, A. N., Chakrabarty, P., Davies, P., & Giasson, B. I. (2020). Tau Ser208 phosphorylation promotes aggregation and reveals neuropathologic diversity in Alzheimer's disease and other tauopathies. *Acta Neuropathologica Communications*, *8*, 88. https://doi.org/10.1186/s40478-020-00967-w 10.1186/s40478-020-00967-w

Xiao, Z. C. M. (2016). Oligodendrocytes and Alzheimer's disease. *International Journal of Neuroscience*, *126*(2), 97–104.

Yanai, T., Masegi, T., Kawada, M., Ishikawa, K., Fukuda, K., Yamazoe, K., Iwasaki, T., Ueda, K., & Goto, N. (1994). Spontaneous vascular mineralization in the brain of cows. *Journal of Comparative Pathology*, *111*, 213–219. https://doi.org/10.1016/S0021-9975(05)80053-2 10.1016/S0021-9975(05)80053-2

Yanai, T., Masegi, T., Ueda, K., Manabe, J., Teranishi, M., Takaoka, M., Matsunuma, N., Fukuda, K., & Goto, N. (1993). Spontaneous globoid mineralization in the cerebellum of rats. *Journal of Comparative Pathology*, *109*, 447–451. https://doi.org/10.1016/S0021-9975(08)80308-8 10.1016/S0021-9975(08)80308-8

Yanai, T., Yamoto, T., Manabe, J., Takaoka, M., & Matsunuma, N. (1987). X-ray microanalysis of mineralization in the thalamus of aged mice. *Nihon Juigaku Zasshi*, *49*(5), 920–922. https://doi.org/10.1292/jvms1939.49.92010.1292/jvms1939.49.920

Youssef, S. A., Capucchio, M. T., Rofina, J. E., Chambers, J. K., Uchida, K., Nakayama, H., & Head, E. (2016). Pathology of the aging brain in domestic and laboratory animals, and animal models of human neurodegenerative diseases. *Veterinary Pathology*, *53*(2), 327–348. https://doi.org/10.1177/0300985815623997 10.1177/0300985815623997

Zecca, L., Tampellini, D., Gerlach, M., Riederer, P., Fariello, R. G., & Sulzer, D. (2001). Substantia nigra neuromelanin: Structure, synthesis, and molecular behaviour. *Molecular Pathology*, *54*(6), 414–8.

Zhu, X., Raina, A. K., Perry, G., & Smith, M. A. (2004). Alzheimer's disease: The two-hit hypothesis. *Lancet Neurology*, *3*(4), 219–226. https://doi.org/10.1016/S1474-4422(04)00707-0 10.1016/S1474-4422(04)00707-0

How to cite this article: Corey, T. M., Illanes, O., Lawrence, M., Perez, S. E., Liddie, S., & Callanan, J. J. (2023). Naturally occurring histological findings and Alzheimer's-like pathology in the brain of aging African green monkeys (*Chlorocebus sabaeus*). *Journal of Comparative Neurology*, 1–23. https://doi.org/10.1002/cne.25494